Gas hydrate petroleum systems: What constitutes the "seal"?

Junbong Jang[1], William F. Waite[2], and Laura A. Stern[3]

Abstract

The gas hydrate petroleum system (GHPS) approach, which has been used to characterize gas hydrates in nature, uses three distinct components: a methane source, a methane migration pathway, and a reservoir that not only contains gas hydrate, but also acts as a seal to prevent methane loss. Unlike GHPS, a traditional petroleum system (PS) approach further distinguishes between the reservoir, a unit with generally coarser sediment grains, and a separate overlying seal unit with generally finer sediment grains. Adopting this traditional PS distinction in the GHPS approach facilitates assessments of reservoir growth and production potential. The significance of the seal for the formation of a gas hydrate reservoir as well as for efficiency in methane extraction from the reservoir as an energy resource is evident in findings from recent offshore field expeditions, such as India's second National Gas Hydrate Program expedition (NGHP-02). In regard to gas hydrate-bearing reservoir formations, the NGHP-02 gas chemistry data indicate a primarily microbial methane source. Fine-grained seal sediment in contact with coarser grained reservoir sediment can facilitate that microbial methane production. Logging-while-drilling and sediment core data also indicate that the overlying fine-grained seal sediment is less permeable than the underlying, highly gas hydrate-saturated reservoir sediment. The overlying seal's capacity to act as a low-permeability boundary is important not only for preventing methane migration out of the reservoir over time, but also for preventing water invasion into the reservoir during methane extraction from the reservoir. Ultimately, the presence of an overlying, fine-grained, low-permeability "seal" influences how gas hydrate initially forms in a coarse-grained reservoir and dictates how efficiently methane can be extracted as an energy resource from the gas hydrate reservoir via depressurization.

Introduction

Methane gas hydrate is a naturally occurring solid formed from methane and water (Sloan and Koh, 2007) that is stable at the moderate temperatures and elevated pressures found primarily in marine continental slope sediments and within or beneath permafrost-associated sediments (Kvenvolden, 1993; Collett et al., 2009). Methane gas hydrate, referred to here as gas hydrate, is inferred to exist in quantities large enough to represent a potential global energy resource (Boswell and Collett, 2011; Johnson, 2011; Wallmann et al., 2012). Like other hydrocarbon energy resources, gas hydrate occurrences have been described in terms of the petroleum system (PS) approach, albeit with a modification described below (Collett, 1995; Frye, 2008; Collett et al., 2009; Max and Johnson, 2014).

The traditional PS approach has four elements (Magoon, 1988): (1) a source or sediment interval in which hydrocarbons are generated; (2) migration pathways, which are permeable conduits through which hydrocarbons can migrate from a source into a reservoir sediment unit; (3) a reservoir, generally a coarse-grained sediment unit with a permeable pore-space network capable of holding hydrocarbons; and (4) an overlying seal of generally fine-grained, impermeable sediment capable of retaining the hydrocarbons within the reservoir unit (Ulmishek, 1988). In contrast, the modified gas hydrate petroleum system (GHPS) has commonly been considered to have only three distinct elements, differing from the traditional PS in that the gas hydrate reservoir unit is itself considered to be the seal (Collett and Kvenvolden, 1988; Max and Johnson, 2014). This modification reflects the significant permeability reduction that occurs as solid gas hydrate forms and builds to higher gas hydrate saturations within the reservoir unit (Rempel and Buffett, 1997; Nimblett and Ruppel, 2003).

High gas hydrate saturations in a coarse-grained reservoir can unquestionably cause the effective permeability

[1]Integrated Statistics Inc., Contracted to U.S. Geological Survey, Woods Hole, Massachusetts, USA; presently Department of Civil Engineering, Dong-A University, Busan, South Korea. E-mail: jjang@contractor.usgs.gov.
[2]U.S. Geological Survey, Woods Hole, Massachusetts, USA. E-mail: wwaite@usgs.gov.
[3]U.S. Geological Survey, Menlo Park, California, USA. E-mail: lstern@usgs.gov.

Manuscript received by the Editor 20 February 2019; revised manuscript received 4 December 2019; published ahead of production 09 January 2020; published online 2 March 2020. This paper appears in *Interpretation*, Vol. 8, No. 2 (May 2020); p. T231–T248, 11 FIGS.
http://dx.doi.org/10.1190/INT-2019-0026.1. © 2020 Society of Exploration Geophysicists and American Association of Petroleum Geologists. All rights reserved.

Downloaded from https://pubs.geoscienceworld.org/interpretation/article-pdf/doi/10.1190/INT-2019-0026.1/4960317/int-2019-0026.1.pdf?casa_token=CeuYDf8A8V4AAAAA:dcWyYhgKtzGllWkcLSwDi9X2CCPeCCKpldR4zP
by USGS Library user

(permeability to water in the presence of gas hydrate k_{eff}) to be orders of magnitude lower than the intrinsic permeability (the permeability to water in the absence of gas hydrate k_{int}). Values of k_{eff} in naturally occurring, coarse-grained, gas hydrate reservoir sediments recovered as pressure cores have been found to range between approximately 1 and 100 mD (mD = millidarcy = 9.869×10^{-16} m^2), with corresponding k_{int} values of approximately 1000–10,000 mD (Konno et al., 2015; Priest et al., 2015, 2019; Santamarina et al., 2015; Boswell et al., 2019b; Yoneda et al., 2019).

In spite of the capacity for gas hydrate to dramatically reduce permeability within the coarse-grained reservoir unit, overlying fine-grained sediment is likely providing the limiting permeability for fluid flow. For example, the permeability of fine-grained sediment overlying a significant gas hydrate reservoir in the Krishna-Godavari (KG) Basin, offshore eastern India (Moridis et al., 2019; Waite et al., 2019a), was measured by three different laboratories using a range of direct and inferred measurement techniques and found to range between 0.012 and 0.052 mD (Dai et al., 2019; Jang et al., 2019a; Priest et al., 2019), two orders of magnitude below the lowest typical k_{eff} measured on gas hydrate-bearing pressure cores in the NGHP-02 program (Yoneda et al., 2019).

The low permeability of an overlying, fine-grained layer relative to an underlying, highly gas hydrate-saturated reservoir points to the importance of considering the overlying sediment as the functional seal element in a GHPS approach. The present study uses examples from the NGHP-02 expedition to illustrate the importance of the overlying sediment's seal characteristics in facilitating the accumulation of gas hydrate in the reservoir and the efficiency with which methane can be extracted from the reservoir as an energy resource. This study recommends specifically testing and characterizing the overlying sediment as a traditional seal unit for the underlying gas hydrate reservoir.

Geologic setting

This study used field data from India's second National Gas Hydrate Program expedition (NGHP-02), which collected seismic, logging, and coring data to investigate natural gas hydrate in the KG Basin in the Indian Ocean as a potential gas resource (Kumar et al., 2019; Shukla et al., 2019b). The NGHP-02 expedition found thick, highly gas hydrate-saturated reservoirs. Based on remote sensing and core measurement data collected during the expedition, reservoir formation processes have been inferred (Dixit et al., 2019; Ijiri et al., 2019; Kinoshita et al., 2019; Saito et al., 2019; Collett et al., 2019), and reservoir production has been modeled to estimate the potential gas production rates (Konno et al., 2019; Moridis et al., 2019; Myshakin et al., 2019).

Among the NGHP-02 study locations (Figure 1), two distinct geologic structures in the KG Basin were selected as sites for this work to show the significance of the overlying fine-grained sediment's role as a seal for the underlying coarser grained gas hydrate-bearing reservoir. As can be seen from the seismic data in Figures 2 and 3, the selected sites show strong seismic reflections (e.g., 3.7–3.8 ms two-way traveltime, approximately 270–290 mbsf in Figure 2; 210–270 mbsf in Figure 3) indicating coarse-grained units hosting gas hydrate, but the geologic structures differ in the two areas (Collett et al., 2019; Jang et al., 2019b; Shukla et al., 2019a, 2019b; Waite et al., 2019a). Detailed descriptions of the geologic history that created the gas hydrate reservoir structures are provided by Collett et al. (2019), Radhakrishna et al. (2012), and Singh (2014). For the purpose of this study, only the geometry and characteristics of the system structures themselves are discussed: Area B has an anticline and syncline structure (Figure 2), whereas Area C has a channel-levee system (Figure 3). In each case, the primary coarse-grained gas hydrate reservoir underlies a finer grained interval. As discussed in this work, differences in the overlying sediment composition, depositional environment, and deformational history combine to cause intersite variations in the sealing properties of the sediment overlying the primary gas hydrate-saturated reservoir layers.

Methods

Downhole and laboratory studies on material collected from sites NGHP-02-16 and -23 in Area B (Figure 2) and sites NGHP-02-08 and -09 in Area C (Figure 3) are used to compare the impact of overlying fine-grained sediment seals on two gas hydrate reservoir structures.

Field measurements

NGHP-02 was a comprehensive project, from which several insights can be drawn from regional seismic data to establish the geologic structure (Collett et al., 2019; Shukla et al., 2019a, 2019b). More insights can be drawn from geochemical analyses of gas and pore water recovered from gas hydrate-bearing pressure cores to infer the methane source for the systems studied here (Holland et al., 2019; Ijiri et al., 2019; Kida et al., 2019). Additionally, logging-while-drilling (LWD) data and core-based measurements collected during NGHP-02 are used to identify and characterize the fine-grained seal layers and the underlying primary gas hydrate-bearing reservoirs. The downhole LWD profiles used in this work are the calculated density-porosity, nuclear magnetic resonance (NMR) estimates of permeability, P-wave velocity V_P, resistivity-based gas hydrate saturation estimates, and clay mineral, quartz-feldspar-mica (QFM) content (Jang et al., 2019b; Waite et al., 2019a).

Although the LWD gamma ray log is often used to characterize the downhole lithology, Areas B and C are characterized by anomalous gamma results that obscure the in situ lithology. Typically, fine-grained sediment is characterized by higher gamma ray responses because those lithologies have higher concentrations of

Downloaded from https://pubs.geoscienceworld.org/interpretation/article-pdf/doi/10.1190/INT-2019-0026.1/4960317/int-2019-0026.1.pdf?casa_token=CeuYDf8A8V4AAAAA:dcWyYhgKtzGllWkcLSwDi9X2CCPeCCKpldR4zP
by USGS Library user

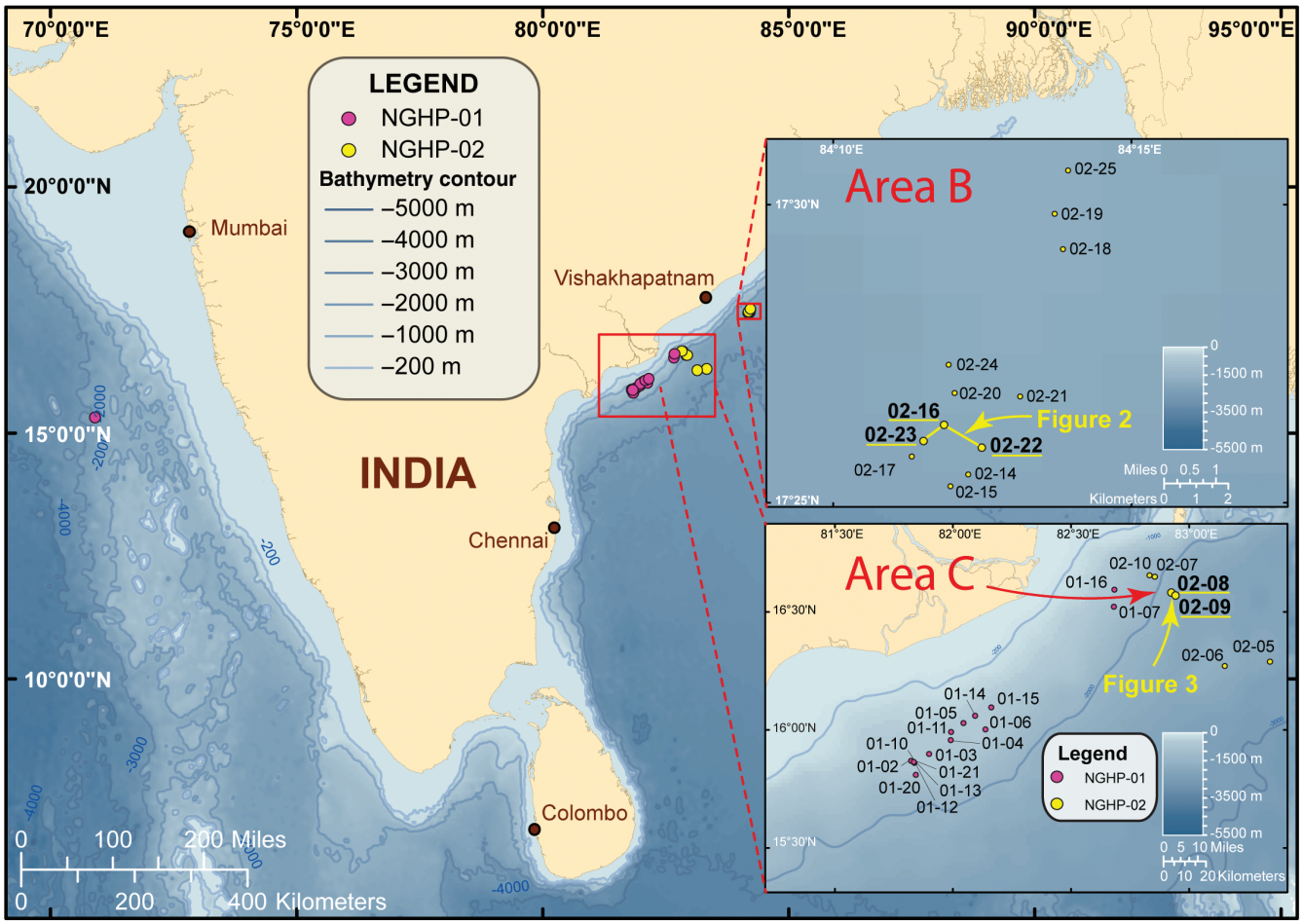

Figure 1. Site locations for the National Gas Hydrate Program of India expeditions NGHP-01 (red dots, Collett et al., 2014) and NGHP-02 (yellow dots). Upper inset: Area B cored the crest of a buried anticline at sites NGHP-02-16, -17, and -23. Site NGHP-02-22 is on the flank of the anticline. The seismic line shown in Figure 3 is indicated in yellow. Lower inset: Area C is in the upper right portion of the inset, with the two channel levee deposit sites (NGHP-02-08, -09) highlighted. The seismic line shown in Figure 4 runs from site NGHP-02-08 to site NGHP-02-09.

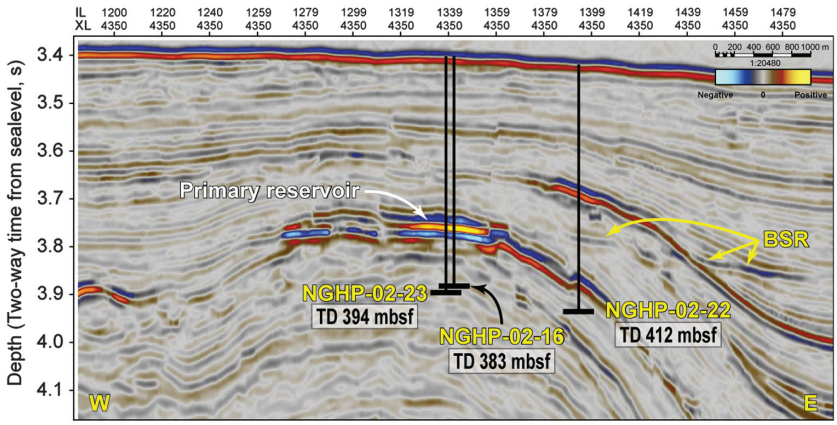

Figure 2. Seismic data along a generally west-to-east transect across an anticlinal structure in Area B. The primary gas hydrate accumulation is characterized by the bright reflectors at the anticline crest, just above the BSR. Sites NGHP-02-16 and -23 penetrate the primary reservoir at the anticline crest (Shukla et al., 2019a, 2019b). Site NGHP-02-16-22 is on the anticline flank, and, as indicated by its penetration of the dipping reflections, it provides information about the primary reservoir's coarse-grained sediment layer where it extends below the base of gas hydrate stability. Total depth (TD) values are given for each well, but the well visualizations are approximate because the vertical axis is in traveltime rather than in depth. The American –90° polarity convention is used here, with a negative (blue) response just above the seafloor and a positive (red) response just below the seafloor. See Shukla et al. (2019a) for additional waveform and amplitude details.

Downloaded from https://pubs.geoscienceworld.org/interpretation/article-pdf/doi/10.1190/INT-2019-0026.1/4960317/int-2019-0026.1.pdf?casa_token=CeuYDf8A8V4AAAAA:dcWyYhgKtzGllWkcLSwDi9X2CCPeCCKpldR4zP
by USGS Library user

radioactive minerals (Adolph et al., 2005). Areas B and C, however, have sand-rich layers with concentrations of mica and biotite high enough to generate gamma ray responses that are higher than those of the adjacent fine-grained material (Collett et al., 2019; Jang et al., 2019b). In this work, the QFM log is used instead to provide qualitative insight about the downhole lithology.

Shipboard pressure core analyses of intact gas hydrate-bearing sediment included V_P, X-ray imagery, as well as gas hydrate saturation measured using the depressurization method (Holland et al., 2019). Depressurized cores, which no longer contain gas hydrate, were used for conventional core analyses, including porosity, grain size, grain density, and grain morphology (Jang et al., 2018, 2019a, 2019b; Waite et al., 2018, 2019a).

Postexpedition laboratory measurements

We conducted laboratory experiments with conventional cores and pressure cores to characterize the fine-grained seal sediments. Laboratory characterization of conventional cores included sediment grain size, as well as morphology analyses using optical and scanning-electron microscopy (SEM) (see the details in Jang et al., 2019b). The pressure core analyses were conducted using pressure core characterization tools while maintaining pressures and temperatures within the gas hydrate stability conditions to preserve in situ gas hydrate (pressure core characterization tools, described by Santamarina et al. 2012). For this work, compressibility and permeability were measured at the in situ vertical effective stress (see the details in Jang et al., 2019a).

Results and analyses

The properties of fine-grained sediment overlying a gas hydrate reservoir are largely ignored in GHPS, beyond considering that the sediment permeability is zero, particularly when considering production models for extracting methane from gas hydrate (Ajayi et al., 2018; Konno et al., 2019). The benefits of considering the reservoir seal unit as a distinct system element are introduced here with data from NGHP-02 Areas B and C, then discussed further in the "Implications" section. To highlight the overlying sediment properties, results are presented within the framework of a traditional PSs approach, which considers the sources, migration pathways, coarse-grained reservoirs, and fine-grained seals.

NGHP-02 Area B, gas hydrate at the crest of an anticline

As indicated in Figures 2 and 4, sites NGHP-02-16 and -23 penetrate two types of gas hydrate occurrences at the anticline crest in Area B. As summarized by Collett et al. (2019), the arrangement of the Area B sediments likely results from a series of large-scale mass transport deposits (MTDs). At the location of sites NGHP-02-16 and -23 in deep water near the toe of the continental slope, the MTD sediment would have likely disaggregated, allowing the coarser grained sediment to settle out prior to the fine-grained MTD components. Subsequent slope-toe thrusting folded the sediment into the anticline that peaks around sites NGHP-02-16 and -23 and slopes downward through site NGHP-02-22 (Figure 2) (Saito et al., 2019; Shukla et al., 2019b; Collett et al., 2019). LWD and core-based measurements (Figure 4) indicate lithologic differences between the shallower seal sediment, some of which contains gas hydrate-filled fractures, and the deeper reservoir interval, which contains pore-occupying gas hydrate.

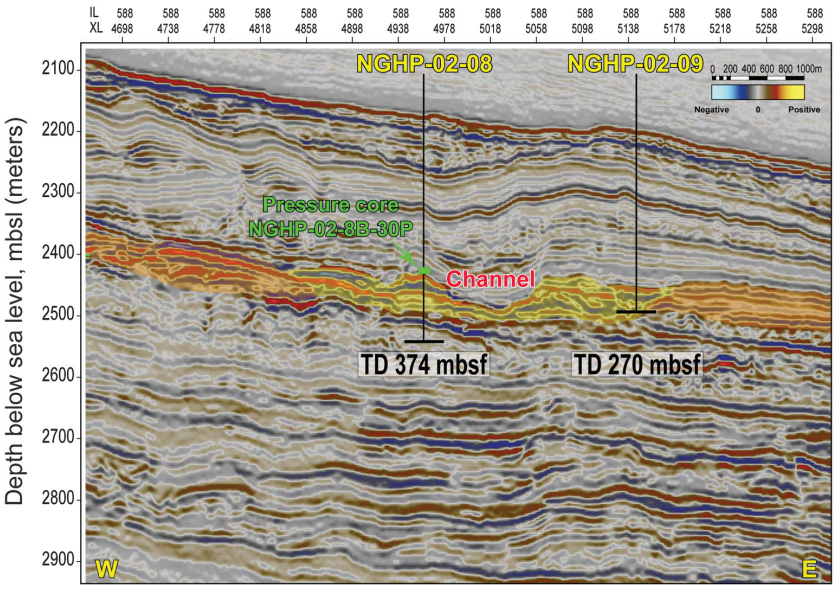

Figure 3. Seismic data along a transect cutting across a channel-levee system in Area C. Yellow shading indicates coarser grained levee sediment deposits that form the primary gas hydrate reservoirs near the channel. Orange shading indicates finer grained levee sediment deposited farther from the channel. Locations of sites NGHP-02-08 and -09 are shown along with their TD values. Site NGHP-02-09 had to be abandoned prior to penetrating the primary gas hydrate reservoir (Kumar et al., 2019). Location of pressure core NGHP-02-8P-30P shows it is from the primary reservoir's overlying seal layer. The American polarity convention is used here, with a positive (red) response just above the seafloor and a negative (blue) seafloor response. See Shukla et al. (2019a) for additional waveform and amplitude details.

Methane source

For the full range of cored depths, gas recovered from gas hydrate-bearing pressure cores had C_1/C_{2+} (ratio of methane to ethane and other higher hydrocarbons) values that exceeded 1000 (Dixit et al., 2019; Kida et al., 2019). Additionally, the stable carbon isotopic ratios ($\delta^{13}C$) of the recovered methane were also light, between −60‰ and −75‰ (Dixit et al., 2019; Kida et al., 2019).

Downloaded from https://pubs.geoscienceworld.org/interpretation/article-pdf/doi/10.1190/INT-2019-0026.1/4960317/int-2019-0026.1.pdf?casa_token=CeuYDf8A8V4AAAAA:dcWyYhgKtzGllWkcLSwDi9X2CCPeCCKpldR4zP
by USGS Library user

These characteristics indicate that gas at the anticline has a microbial origin (Collett et al., 2019; Dixit et al., 2019; Kida et al., 2019), which is supported by elevated methanogen concentrations cultured from sediments associated with the primary Area B gas hydrate reservoir by Tripathi et al. (2019).

Methane migration pathways

Although LWD permeability measurements were not made at sites NGHP-02-16 or -23, physical properties from LWD and recovered sediments (Figure 4) indicate that the coarsest material at these two sites corresponds to the primary gas hydrate reservoir (approximately 270–300 meters below seafloor, mbsf). This coarse interval has the highest intrinsic permeability in the system, discussed further in the next section. As indicated in Figure 2, the bright seismic reflections signifying this coarse-grained sediment layer follow the geologic structure down the flank of the anticline. Data from site NGHP-02-22, an LWD and coring site located on the anticline flank, verified that this coarse-grained interval did in fact extend below the bottom-simulating reflector (BSR) (Jang et al., 2019b; Kumar et al., 2019).

Considering the higher permeability of this coarse-grained layer relative to the adjacent fine-grained sediments, along with its anticlinal geometry, the coarse-grained layer has been interpreted as an advective pathway for methane to migrate from below the BSR up into the primary gas hydrate reservoir at the anticline crest (Jang et al., 2019b; Saito et al., 2019). This interpretation is supported by the pore-water decrease of Cl^- with depth to near constant values (Ijiri et al., 2019). The profile shape is due to upward migration of low-Cl^- fluid into and through the primary gas hydrate reservoir at the anticline crest (Ijiri et al., 2019). Mass-balance calculations by Ijiri et al. (2019) based on pore-water Cl^- concentrations and isotopic measurements of oxygen and deuterium from above and below the primary coarse-grained gas hydrate reservoir indicate only 10%–20% of the upward advecting fluid is trapped in the reservoir interval.

The advecting fluid carries microbially sourced methane up to the primary gas hydrate-bearing reservoir at the Area B anticline crest (Dixit et al., 2019). Some of that methane is recycled from gas hydrate that was previously pushed below the base of gas hydrate stability due to sedimentation (Paull et al.,

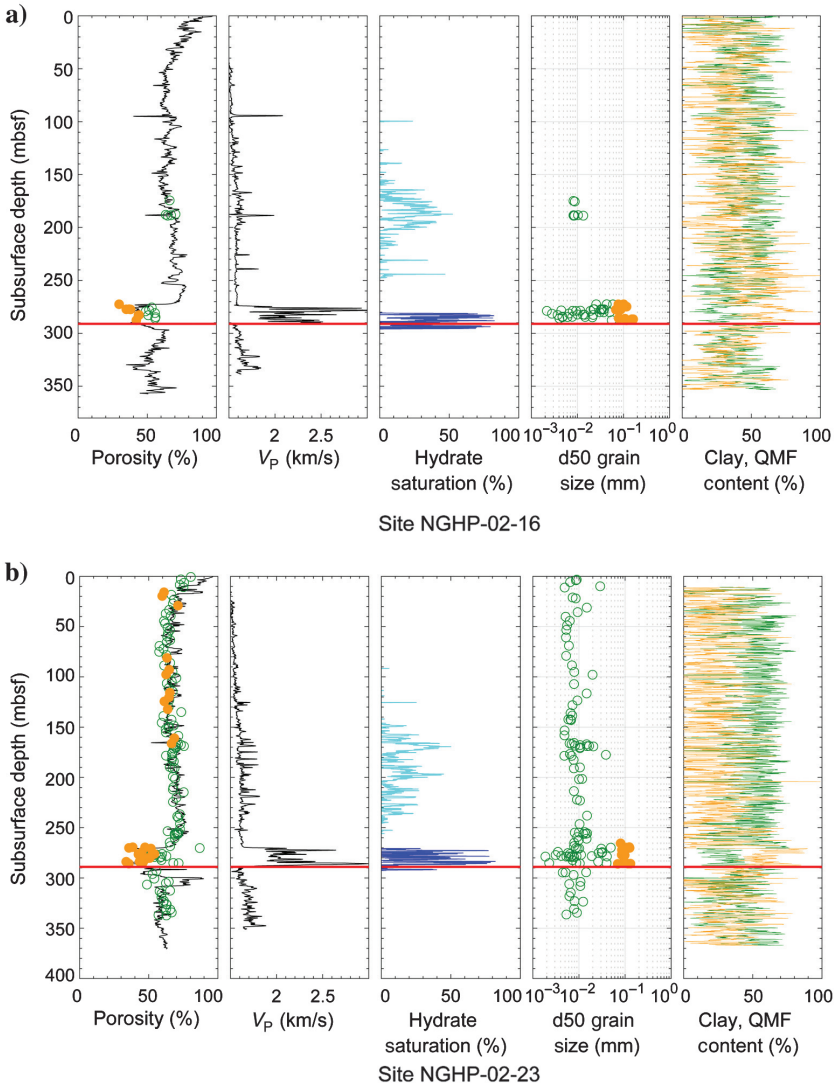

Figure 4. Physical properties from LWD and sediment core measurements for sites NGHP-02-16 and -23 in (a and b), respectively. Downhole traces are from LWD, whereas point data (open and filled circles) are from laboratory measurements of recovered conventional and pressure cores. Green curves and open circles represent fines (which are also represented by the clay mineral content in the rightmost panel), and orange curves and solid circles represent sand (which is also represented by the QFM content in the rightmost panel). The LWD porosity (black curve) is a density-based porosity calculated from the LWD bulk density log and grain density measurements on the recovered sediment. The Archie-based gas hydrate saturation (calculation parameters for each site are given in Table 3 of Collett et al., 2019) use Ecoscope P40H phase resistivity data. In combination with the V_P and mineral content results, the LWD resistivity data indicate two gas hydrate morphologies: generally pore-occupying hydrate in the primary coarse-grained reservoir (the dark blue curve, which correlates with V_P well above the background values and with reduced clay content) and primarily gas hydrate-filled fractures in fine-grained sediment (the light blue curve, which is not correlated with V_P or with reduced clay content). As noted by Collett et al. (2019), gas hydrate saturations in the gas hydrate-filled fracture intervals are likely overestimated due to the vertically oriented fractures (Cook et al., 2010). The red horizontal line is the base of the gas hydrate occurrence zone (Waite et al., 2019b). Figure modified from Jang et al. (2019b).

Downloaded from https://pubs.geoscienceworld.org/interpretation/article-pdf/doi/10.1190/INT-2019-0026.1/4960317/int-2019-0026.1.pdf?casa_token=CeuYDf8A8V4AAAAA:dcWyYhgKtzGllWkcLSwDi9X2CCPeCCKpldR4zP
by USGS Library user

1994; Dixit et al., 2019), but some of the methane is microbially sourced from below the reservoir, in the interval between approximately 300 and 1000 mbsf (Collett et al., 2019; Dixit et al., 2019).

Methane migrating up the prominent coarse-grained unit, past site NGHP-02-22 and into the gas hydrate-bearing reservoir at sites NGHP-02-16 and -23 (Figure 2), is more likely to be dissolved-phase methane because there is a water-bearing contact at the base of the gas hydrate in the primary reservoir on this side of the anticline (Shukla et al., 2019b; Waite et al., 2019b). Methane is more likely to be present as a free gas phase below the BSR on the opposite side of the anticline (Figure 2, at the inline 1279 location) (Shukla et al., 2019b).

Additionally, vertical fractures are observed at the anticline crest, predominantly between approximately 150 and 240 mbsf (Saito et al., 2019). These fractures are interpreted to have formed as a result of extensional flexure that occurred during the folding that created the anticlinal structure (Saito et al., 2019). In combination with the seismically imaged vertical faults extending through the primary gas hydrate reservoir (Shukla et al., 2019b), the vertical fractures provide additional migration pathways for methane at the anticline crest to migrate vertically out of the primary gas hydrate reservoir and into the overlying seal sediment.

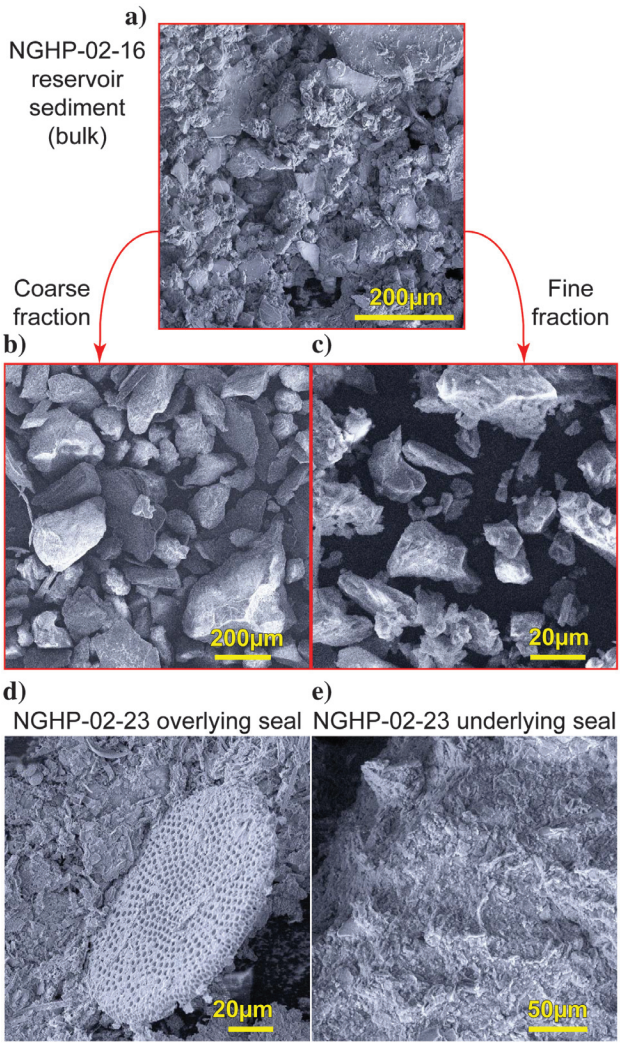

Figure 5. The SEM images of grains from conventional cores at the anticline crest in Area B. (a-c) Grains from a sandy reservoir layer in the primary gas hydrate reservoir at site NGHP-02-16. The bulk sample of (a) was sieved to obtain separate images of the (b) coarse- and (c) fine-grained fractions. Images (d and e) are, respectively, seal sediments from above and below the primary gas hydrate reservoir at site NGHP-02-23. (d) Diatoms (porous disc) and diatom shards are abundant in the overlying seal sediment but they are not apparent in the underlying seal (e), which shows a mass of clustered clay minerals.

Relationship between reservoir and seal sediment

Figure 4 shows downhole LWD and core measurement data for sites NGHP-02-16 and -23, along with an Archie's law-based estimate of the downhole distribution of gas hydrate. Above approximately 250 mbsf, gas hydrate occurs primarily as gas hydrate-filled fractures in fine-grained sediment. Between approximately 270 and 300 mbsf, gas hydrate occurs primarily as a pore-occupying phase in the coarse-grained sediments in the gas hydrate reservoir.

Figure 5 shows particle shapes from the sandy, primary reservoir at the anticline crest in Area B, in comparison to overlying and underlying seal sediment. The sandy reservoir has equidimensional, angular particles in its coarse and fine fractions (Figure 5b and 5c), reflecting the low clay mineral content measured via LWD in this interval (Figure 4). The overlying seal contains clay minerals (approximately 30%) with significant microfossil (diatom) concentrations (approximately 20%), whereas the underlying sediment contains clay minerals (approximately 25%) without abundant microfossils. Unlike the equidimensional, distinct particles in the sandy reservoir (Figure 5b and 5c), fines in the seals are strongly influenced by electrostatic interparticle interactions and therefore tend to cluster or clump as they dry prior to imaging (Figure 5d and 5e). There is also a distinct porosity difference between the reservoir and seal (Figure 4): The sediment core porosity in the sandy primary gas hydrate reservoir sediment is approximately 40% (Figure 4, solid orange circles in the porosity panel), which is close to the loose packing conditions for sandy sediment [the median particle size (d_{50}) of the primary gas hydrate reservoir sediment is up to 100 µm, which is classified as a very fine sand]; the approximately 70% porosity observed in the overlying and underlying sediments is likely due to platy particles such as clay minerals and, in the overlying seal, the diatoms. The high apparent porosity in the reservoir interval recorded by LWD (Figure 4, the black curve in the porosity panel) is due to borehole washout and does not reflect the in situ porosity.

Based on empirical relationships between particle morphology and permeability (Amer and Awad, 1974;

Downloaded from https://pubs.geoscienceworld.org/interpretation/article-pdf/doi/10.1190/INT-2019-0026.1/4960317/int-2019-0026.1.pdf?casa_token=CeuYDf8A8V4AAAAA:dcWyYhgKtzGllWkcLSwDi9X2CCPeCCKpldR4zP
by USGS Library user

Carrier, 2003; Chapuis, 2004; Ren and Santamarina, 2018), the intrinsic permeability of the sandy layers of the primary gas hydrate reservoir is inferred to be approximately 1000 mD (1 mD is 9.869×10^{-16} m^2), almost five orders of magnitude higher than the 0.02 mD inferred for the overburden seal layer (Jang et al., 2019a). Even in the presence of gas hydrate, effective permeability measurements by Yoneda et al. (2019) on high gas hydrate-saturation pressure cores (gas hydrate occupying more than 60% of the available pore space) recovered from sites NGHP-02-16 and -23 show that the effective permeability is generally one to three orders of magnitude greater than the intrinsic, hydrate-free permeability inferred for the overlying seal.

However, the overlying seal has a high diatom content (Figure 5d), and this is anticipated to increase the true permeability relative to the inferred value of 0.02 mD given above. Diatoms can increase porosity and permeability because the open structure and the irregular shapes of the numerous diatom shards prevent neighboring fine grains from forming a low-permeability fabric (Kraemer et al., 2000; Spinelli et al., 2004). The LWD porosity logs (Figure 4) show that porosity slightly increases with depth between approximately 50 mbsf and the top of the coarse-grained gas hydrate reservoir near 270 mbsf. The porosity trend does not follow a typical compaction trend with depth because the diatom concentration increases with depth over this range (Jang et al., 2019b) and the diatoms prevent efficient compaction. The presence of diatoms, combined with the near 70% porosity of the seal sediment just above the coarse-grained gas hydrate reservoir, limits the effectiveness of this seal, which allows 80%–90% of the advecting fluids to move up through the gas hydrate-bearing reservoir and into the overlying sediment (Ijiri et al., 2019). This flow can transport methane into the overlying fine-grained sediments, contributing to the observed gas hydrate-filled fractures.

The true seal sediment responsible for preventing the migration of underlying methane may be at shallow depths in the sediment column (50 to approximately 150 mbsf). As discussed by Saito et al. (2019), a network of vertical faults at the crest of the anticline terminates near 150 mbsf, as do the gas hydrate-filled fractures. Between 0 and approximately 150 mbsf, the lack of observable faulting and gas hydrate suggest that the sediment above approximately 150 mbsf provides a competent seal.

NGHP-02 Area C, gas hydrate in a channel/levee deposit

Area C contains a channel/levee system, with coarse-grained levee sediment deposited near the channel (Figure 3) (Collett et al., 2019). These coarse-grained sediments are potentially significant, energy-resource-quality gas hydrate reservoirs (Moridis et al., 2019; Waite et al., 2019a). Sites NGHP-02-08 and -09 are located on opposite sides of the channel. As indicated by Figure 3, site NGHP-02-08 penetrates a local high in the coarse-grained sediment, and site NGHP-02-09 penetrates the coarse-grained sediment slightly off a local high. Cores from these sites provide evidence that the channel/levee system is overlain by primarily fine-grained MTDs (Waite et al., 2019a). Sandy levee deposits are localized near the channel and host thick gas hydrate layers, whereas fine-grained deposits dominate the areas above and away from the channel.

Methane source

Similar to Area B, gas samples from Area C are dominated by isotopically light methane, indicating a primarily microbial origin for the methane in this system (Holland et al., 2019; Kida et al., 2019). Most, if not all, of the methane generation is inferred to occur in the upper 1000 m of sediment (Collett et al., 2019), with methane recycled at the base of gas hydrate stability during sedimentation contributing to the high observed gas hydrate saturations (Paull et al., 1994; Collett et al., 2019; Dixit et al., 2019). Contributions from advective flow bringing methane from below the gas hydrate reservoir is also likely, but these subreservoir sources would also have to be microbial to produce the observed abundance of isotopically light methane (Dixit et al., 2019).

Methane migration pathways

Unlike Area B, where the primary coarse-grained reservoir layer follows an anticline profile and extends down below the BSR to act as a conduit for methane migration, the geologic structure of Area C has no obvious methane conduit into the localized, coarse-grained levee deposits. Moreover, based on the seismic reflection data (Figure 3), Shukla et al. (2019a) conclude that sites NGHP-02-08 and -09 have little to no free gas below the primary gas hydrate reservoirs.

Though faults were not specifically identified near these sites (Shukla et al., 2019a, 2019b), vertical methane migration through permeable fractures or faults that cross through the levee-deposit gas hydrate reservoir cannot be ruled out (Waite et al., 2019a). Relative to the Area B anticline, however, pore-water chlorinity profiles indicate that advection rates are low at sites NGHP-02-08 and -09 (Collett et al., 2019).

It is likely that fine-grained sediment adjacent to the sites NGHP-02-08 and -09 gas hydrate reservoirs contributes microbially generated methane to the gas hydrate reservoir via the diffusive process described by Malinverno (2010) and Cook and Malinverno (2013). Because these reservoirs have a high average as hydrate concentrations over relatively thick intervals (approximately 25 m, Waite et al., 2019a), it is unlikely that the reservoirs were gas hydrate filled purely through diffusive methane transport. As modeled by Nole et al. (2017), diffusive methane transport cannot uniformly fill sands in excess of approximately 10 m thickness to high gas hydrate saturations, so some level of advection is likely required to generate the observed gas hydrate distributions.

Downloaded from https://pubs.geoscienceworld.org/interpretation/article-pdf/doi/10.1190/INT-2019-0026.1/4960317/int-2019-0026.1.pdf?casa_token=CeuYDf8A8V4AAAAA:dcWyYhgKtzGllWkcLSwDi9X2CCPeCCKpldR4zP
by USGS Library user

Relationship between reservoir and seal sediment

As shown in Figure 6, most of the gas hydrate in Area C is concentrated in the primary coarse-grained reservoir (NGHP-02-08: approximately 250–270 mbsf, 30%–70% gas hydrate saturation; NGHP-02-09: approximately 210–270 mbsf, which was the deepest logging depth, approximately 50%–75% gas hydrate saturation). The reservoir sediment is generally much coarser at these sites than was found within Area B (compare Figures 5 and 7). Like in the sediment above the primary Area B gas hydrate reservoir, gas hydrate occurs as gas hydrate-filled fractures in the fine-grained seal sediment of site NGHP-02-08 (e.g., approximately 80–100 mbsf). These gas hydrate-filled fractures occur to a lesser extent at site NGHP-02-08 than in Area B, and these features are absent in the site NGHP-02-09 seal sediment. Differences in the gas hydrate distributions between Areas B and C can be linked in part to the local seal-sediment lithology and in part to the seal sediment depositional history: The Area C sites contain clay-rich, diatom-free seal sediment (compare Figures 5 and 7), and unlike the Area B anticline sediment, the Area C sediments have not been extensively deformed since their deposition.

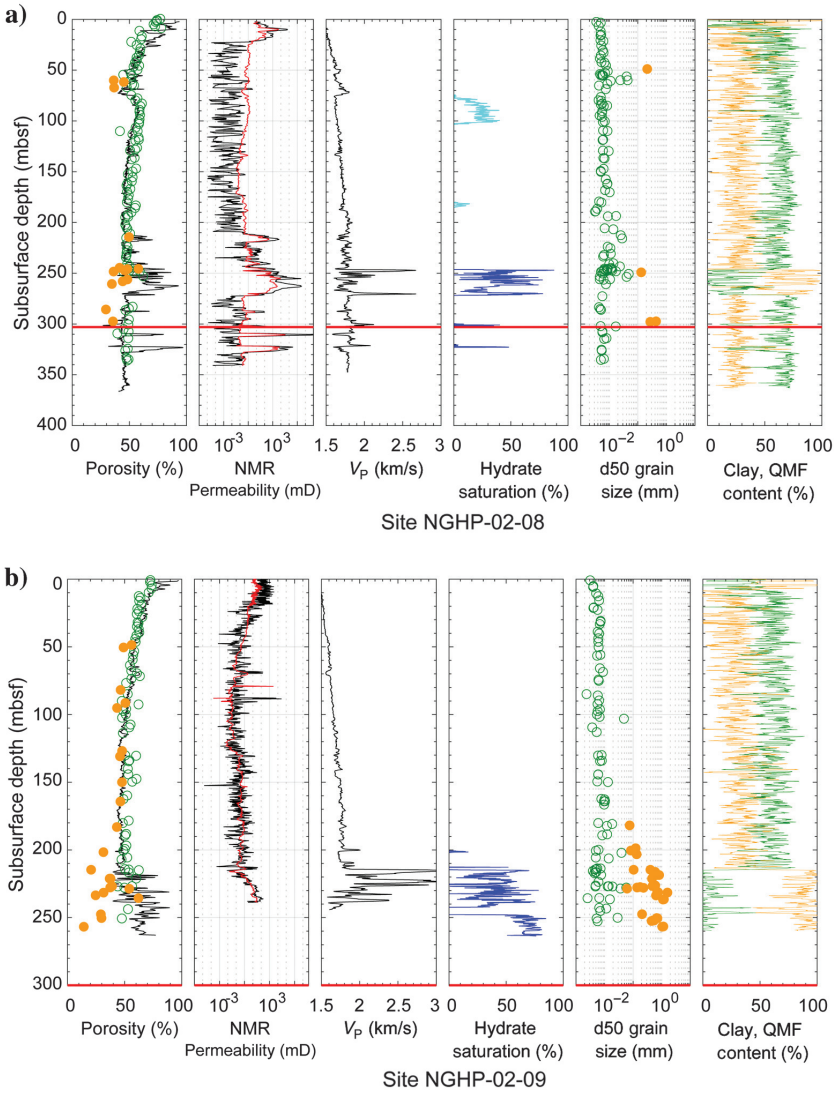

Figure 6. Physical properties from LWD and sediment core measurements for sites NGHP-02-08 and -09 in (a and b), respectively. The legend is identical to Figure 4, with the addition of LWD permeability measurements in the second panel: Downhole traces are from the LWD NMR tool, processed either according to the Timur-Coates approach ($K_{T\text{-}C}$, black) or Schlumberger Doll Research approach (k_{SDR}, red) (described by Fujii et al., 2015). Permeability results for both sites indicate that the fine-grained overlying seal has a lower permeability than the coarse-grained, primary gas hydrate-bearing reservoir. Gas hydrate-filled fractures appear in the seal sediment (light blue in [a]) overlying the primary gas hydrate reservoir at site NGHP-02-08 (dark blue in [a]), but no gas hydrate-filled fractures are apparent in the site NGHP-02-09 overburden (dark blue in [b]). Figure modified from Waite et al. (2019a).

The clay-rich fines above the levee-deposit gas hydrate reservoirs have more classically shaped compaction curves (Figure 6) than those that were observed at the Area B anticline (Figure 4), and the seal porosity is below 50% where the seal contacts the gas hydrate reservoir. As observed in Area B, the core-derived porosity results are lower than the LWD measurement (Figure 6, the solid orange circles and black curve in the porosity panel, respectively), indicating borehole washout during the LWD run that occurred in the gas hydrate reservoir interval.

As shown in Figure 6, the LWD data for Area C include permeability estimates based on the nuclear magnetic resonance (NMR) tool. The NMR permeability profiles show that the permeability is higher, even in the coarse-grained levee sediment where gas hydrate is present and the LWD results are not compromised by borehole washout (Waite et al., 2019a), than it is in the hydrate-free overlying seal.

At site NGHP-02-09, the gas hydrate saturation profile shows gas hydrate being constrained within the coarse-grained, low-clay-content reservoir sediment in a pore-occupying morphology that causes V_P values to increase in correlation with the resistivity-based gas hydrate saturation. At site NGHP-02-08, however, the gas hydrate saturation profile indicates that gas hydrate also fills fractures in the seal layer (Figure 6a, the light blue curve). As anticipated for a fracture-filling gas hydrate interval, V_P is not correlated with the gas hydrate saturation, nor do grain sizes or clay content vary from their background values (Figure 6).

These observations indicate potential differences in the quality of the seal sediments overlying the coarse-grained gas

Downloaded from https://pubs.geoscienceworld.org/interpretation/article-pdf/doi/10.1190/INT-2019-0026.1/4960317/int-2019-0026.1.pdf?casa_token=CeuYDf8A8V4AAAAA:dcWyYhgKtzGllWkcLSwDi9X2CCPeCCKpldR4zP
by USGS Library user

hydrate reservoirs in Area C. The site NGHP-02-08 seal is slightly more permeable than the site NGHP-02-09 seal (Figure 6). Specifically, the NMR-derived k_{SDR} estimate of the overlying seal permeability for site NGHP-02-08 is 26 mD near the gas hydrate reservoir and 0.25 mD at 103–212 mbsf, whereas that of site NGHP-02-09 is 0.16 mD. The site NGHP-02-08 seal appears to allow methane to migrate upward and form gas hydrate-filled fractures in the overlying fine-grained sediment.

The NMR-based permeability estimate, though useful for capturing the permeability change across the transition between the reservoir and seal sediment, overpredicts the seal sediment permeabilities compared with the permeabilities measured directly on recovered sediment (Fujii et al., 2015; Dai et al., 2017). As described below, two suggested sources — measurement technique and measurement resolution — likely contribute in this instance.

NMR-based permeability measurements have no flow direction associated with them, unlike direct, water-flow-based techniques, meaning that the NMR results can be misleading where the permeability is anisotropic. For example, the horizontal permeability measured by water-flow-based techniques is one order of magnitude greater than the vertical permeability for the site NGHP-02-08 fine-grained seal (Dai et al., 2019). If the NMR result provides an average permeability over the various flow directions, it should be higher than the flow-based vertical permeability results.

Vertical measurement resolution is another potential source of the discrepancy between NMR and direct permeability measurements. Though the seal sediment is generally uniform in grain size, thin, mm-to-cm-scale coarser grained layers are also present in Area C (Figure 8). The X-ray and microscope images in Figure 8 show a localized nonuniformity in the pressure-cored sediment. The thin layer near 247.6 mbsf corresponds to a V_P peak and a low-density (white) interval in the X-ray, the combination of which indicates gas hydrate. Microscope images also indicate a distinct discrepancy between the low- and high-V_P sediment. The low-V_P sediment contains fines, such as clay minerals, that cluster during the drying process, rather than remaining as separate grains. The high-V_P sediment contains equidimensional, angular grains that tend to form fabrics with larger pore spaces, which are critical for gas hydrate formation (Uchida et al., 2009; Malinverno, 2010).

Because the core's initial shipboard X-ray and V_P scans located the seal sediment's nonuniformity (Holland et al., 2019; Jang et al., 2019a), the direct flow measurements by Jang et al. (2019a), which used 5–6 cm core subsections,

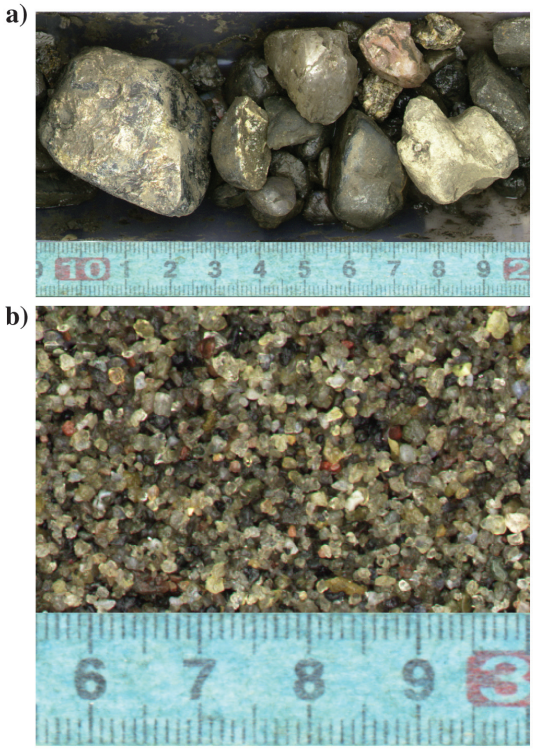

Figure 7. Shipboard natural-light images of depressurized sediments from pressure cores collected from the coarse-grained levee interval from Area C. Scale beneath each image is in centimeters. (a) Site NGHP-02-08, 269.6 mbsf: d_{50} was not measured, but it is visually estimated to be on the order of 1 cm (10,000 μm). (b) Site NGHP-02-09, 257.3 mbsf: d_{50} is 0.11 cm (1100 μm), with a clay content of only 0.3% (Waite et al., 2019a). By comparison, d_{50} is of the order of 100 μm for the coarse-grained reservoir at the crest of the Area B anticline (Jang et al., 2019b).

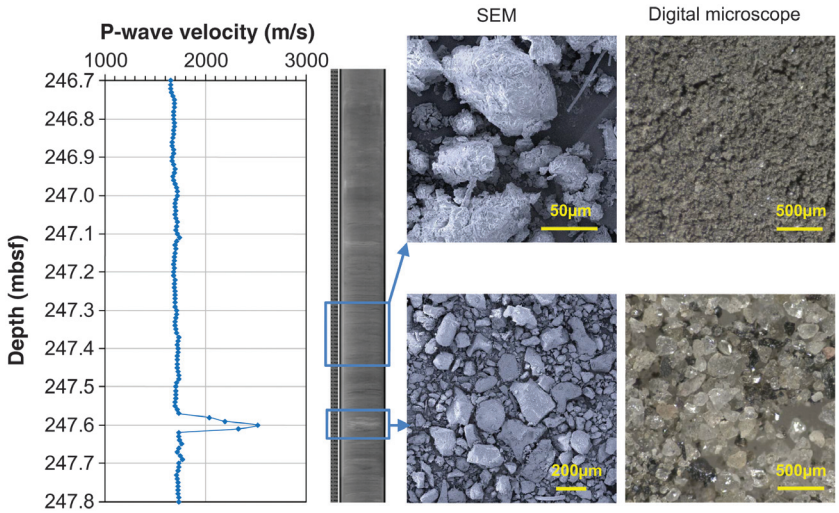

Figure 8. Shipboard P-wave velocity and X-ray image of pressure core NGHP-02-8B-30P, along with microscope images of subsections from the pressure core. The high-velocity anomaly at 247.6 mbsf is taken as an indicator of a thin, gas hydrate-bearing layer. This layer corresponds to the low-density band (lighter color) in the X-ray, and to coarser, lower clay-content sediment. Based on SEM-EDS (energy dispersive spectroscopy) of the thin interbed, the clear grains are quartz, and black grains contain titanium and iron (possibly ilmenite or a member of the pyroxene group).

Downloaded from https://pubs.geoscienceworld.org/interpretation/article-pdf/doi/10.1190/INT-2019-0026.1/4960317/int-2019-0026.1.pdf?casa_token=CeuYDf8A8V4AAAAA:dcWyYhgKtzGllWkcLSwDi9X2CCPeCCKpldR4zP
by USGS Library user

could be positioned specifically to avoid the coarse-grained interval. The NMR resolution, however, is 120 cm in the vertical direction (Collett et al., 2015; Waite et al., 2019a), providing the average permeability of the bulk sediment. The NMR-based technique is therefore susceptible to having thin, coarse-grained layers increase the permeability estimate for the surrounding low-permeability, fine-grained sediment.

As described by Malinverno (2010), the presence of these thin, coarser grained layers embedded in fine-grained sediment may contribute to the presence of gas hydrate observed in the shallower sediment column (Figure 6, the light-blue gas hydrate saturation curve). In the short-range methane migration process described by Malinverno (2010), methane generated microbially in the fine-grained sediment diffuses into adjacent coarse-grained sediment where the lower methane solubility allows gas hydrate to accumulate. Cooler temperatures within the shallower coarser grained layer drive the methane solubility lower than it is near the deeper, warmer reservoir (Zatsepina and Buffett, 1997; Xu and Ruppel, 1999). This enables more of the dissolved methane to be used for gas hydrate formation. Once hydrate forms in localized coarser grained lithologies, gas hydrate-filled fractures such as those observed at site NGHP-02-08 (approximately 80–100 mbsf) can form in the surrounding fine-grained sediment via gas hydrate-induced heave (Daigle and Dugan, 2010). In this interpretation, methane is being sourced locally at the gas hydrate-filled fracture depths, meaning that the seal sediment overlying the primary reservoir at site NGHP-02-08 is not necessarily allowing methane to migrate up and out of the primary gas hydrate reservoir to supply the gas hydrate-filled fractures.

Implications

The GHPS approach essentially ignores the characteristics of sediment overlying a coarse-grained gas hydrate reservoir. This section builds on data from the "Results" section to indicate the insights that are possible by instead applying the traditional PS approach to testing and analyzing gas hydrate reservoirs. The characteristics of fine-grained sediment that overlies or contacts coarse-grained reservoir sediment have implications for gas hydrate formation in the reservoir, as well as for the efficiency of extracting methane as an energy resource from the reservoir.

Gas hydrate formation

Gas hydrate reservoirs are commonly formed from primarily methane (Kvenvolden and Barnard, 1983; Ryu et al., 2009; Yoshioka et al., 2010; Katayama et al., 2016), and microbially derived methane was the dominant guest molecule in the gas hydrate recovered during NGHP-02 (Dixit et al., 2019; Kida et al., 2019). How that microbial methane is sourced into the gas hydrate occurrence interval is site-dependent (Hyndman and Davis, 1992; Marchesi et al., 2001; Malinverno, 2010; Yoshioka et al., 2010), and the exact depths, processes, and rates by which microbial methane generation and subsequent gas hydrate formation occur are actively being investigated (Flemings et al., 2017; Daigle et al., 2018; Grundger et al., 2019; Tripathi et al., 2019; You et al., 2019). Conceptually, however, the presence of fine-grained sediment in contact with coarser grained sediment can facilitate microbial methane formation (D'Hondt et al., 2004), increasing the pore-water methane saturation in the coarse-grained sediment and thereby enhancing the growth of gas hydrate (Malinverno, 2010).

As discussed by Xu and Ruppel (1999), the formation of methane hydrate requires the pore-water methane concentration to exceed the local methane solubility limit. As shown in Figure 9, gas hydrate occurrences lying close to the base of gas hydrate stability require the highest pore-water methane concentration to remain stable or grow. This requirement is satisfied for the primary gas hydrate reservoir at the crest of the Area B anticline from NGHP-02 (Figure 2), where pressure core degassing studies by Holland et al. (2019) demonstrate that methane concentrations exceed the solubility limit, indicating the presence of gas hydrate. The blue arrows in Figure 9 indicate two mechanisms for delivering the necessary methane to a coarse-grained interval: short-range diffusion and short- or long-range advection. Both processes are facilitated by the overlying fine-grained sediment.

Short-range diffusive methane migration from fine-grained sediment into neighboring coarser grained sediment is indicated on the right side of Figure 9 by small blue arrows entering the coarse-grained reservoir. The presence of organic material in the neighboring fine-grained sediment can be used for methanogenesis (Wellsbury et al., 1997), and this microbial methane can diffuse into the coarse-grained interval via the process described by Malinverno (2010).

Short- or long-range advective migration of methane upward along a dipping, permeable, coarse-grained interval is shown in Figure 9 by large blue arrows. This advection can be facilitated by grain-size contrasts. For example, relative to coarse-grained sediment, fine-grained sediment is compressible, and compaction during sedimentation and burial can force methane-rich pore fluids to flow from the fine-grained sediment into a neighboring coarse-grained interval (Daigle et al., 2018). The migration could be short-ranged, occurring in or near the gas hydrate stability zone, or longer ranged as deeper fluids are forced upward relative to the gas hydrate-bearing reservoir by the compaction of fine-grained sediments in the upper approximately 500 mbsf (Berner, 1980). This upward migration of methane toward the gas hydrate stability zone within the more permeable coarse-grained sediment can also include methane recycled from gas hydrate pushed below the base of gas hydrate stability by sedimentation (Paull et al., 1994) and can include methane in the free-gas phase in addition to dissolved-phase methane.

Downloaded from https://pubs.geoscienceworld.org/interpretation/article-pdf/doi/10.1190/INT-2019-0026.1/4960317/int-2019-0026.1.pdf?casa_token=CeuYDf8A8V4AAAAA:dcWyYhgKtzGllWkcLSwDi9X2CCPeCCKpldR4zP
by USGS Library user

The comparatively high methane concentrations and low permeability of a fine-grained overburden relative to an underlying coarse-grained interval limits the diffusion and advection of methane out of the coarse-grained layer (Clennell et al., 1999; Henry et al., 1999; Malinverno, 2010). Consequently, the pore-water methane concentration can be enhanced in the coarse-grained interval, promoting gas hydrate growth when the methane concentration reaches the solubility limit (Figure 9, right side, the solid yellow and white curves, respectively).

If the fine-grained overburden permeability is high, perhaps due to fractures, faulting, or high concentrations of diatoms as observed at the Area B anticline crest, the capability to restrict methane migration out of the coarse-grained sediment can be limited (Figure 9, the left side, small blue arrows). As a consequence, the methane concentration may not be able to reach the solubility limit in the coarse-grained interval, resulting in no gas hydrate generation (Figure 9, the left side, dashed yellow curve).

Though much of the discussion here is centered on a seal's interaction with dissolved-phase methane, an overlying fine-grained layer can also act as a free-gas seal because the relatively small pore-throat sizes in fine-grained sediment require larger gas pressures for gas to invade the pores than is required in the underlying coarse-grained interval (Clennell et al., 1999; Henry et al., 1999; Liu and Flemings, 2011; Meyer et al., 2018). Gas hydrate formation from free methane gas trapped in a coarse-grained reservoir is thought to have created many of the Arctic permafrost-associated gas hydrate occurrences (Boswell et al., 2011; Collett et al., 2011; Dai et al., 2011) and may also contribute to marine gas hydrate accumulations (Liu and Flemings, 2006; You and Flemings, 2018).

As the trapped gas pressure increases below a fine-grained seal, however, gas can fracture and invade the overlying seal (Liu and Flemings, 2007; Jain and Juanes, 2009), forming gas- and hydrate-filled chimneys (Liu and Flemings, 2007). However, with a potential exception offshore western Japan (Matsumoto et al., 2017), gas chimneys are not thought to be as likely as gas hydrate-bearing coarse-grained reservoirs to be economically viable as energy resources (Boswell and Collett, 2011).

For simplicity, Figure 9 shows only the fine-grained sediment above and below the coarse-grained interval. As indicated in Figure 4 for NGHP-02 Area B, the primary coarse-grained, gas hydrate-bearing interval is interbedded with additional fine-grained units (Jang et al., 2019b). These fine-grained interbeds can contribute to the generation of methane that can diffuse into the coarse-grained intervals and can be used for gas hydrate formation. As suggested by D'Hondt et al. (2004), the interfaces between fine- and coarse-grained material can be particularly active regions for methanogenesis. This is because pore water at and near the interfaces is well-suited for hosting electron donors (such as acetate) from the fine-grained sediment and electron acceptors (such as hydrogen [Marchesi et al., 2001] and dissolved iron and manganese species [D'Hondt et al., 2004]) from fluid flow through the more permeable coarse-grained sediment. Within this methane transport process, gas hydrate formation can act as a methane sink, sequestering a microbial product (methane) to allow methanogenesis to continue more efficiently (Chong et al., 2002).

Even after gas hydrate forms, the seal's capacity to limit methane loss from the reservoir is critical to the continued existence of the gas hydrate. If the seal is compromised, methane can escape the reservoir, pore water methane concentrations will drop below the solubility limit, and gas hydrate within the reservoir will dissolve. As an extreme example, gas hydrate in pressure

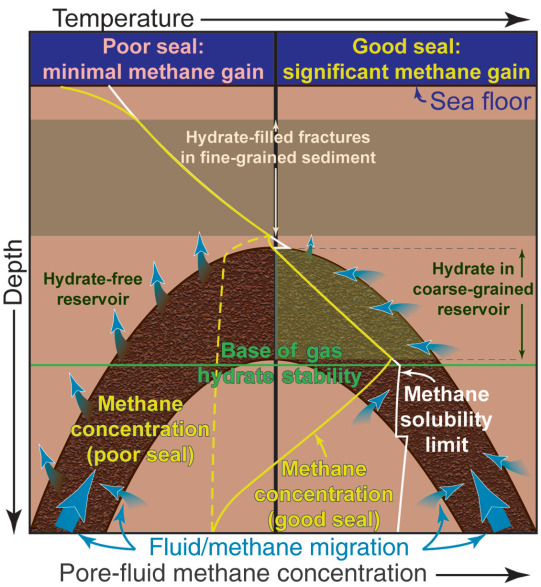

Figure 9. Idealized anticlinal coarse-grained reservoir (the stippled arch), bounded by permeable, low-clay-content, low-quality seal sediment (the left-hand side), or by low-permeability, fine-grained, high-quality seal sediment (the right-hand side). For a poor seal, compromised perhaps by faults, fractures, or high diatom concentrations (the left-hand reservoir), methane is not well-confined (the blue arrows indicate methane loss from the reservoir), so the pore-water methane concentration (the yellow dashed curve) does not reach the methane solubility limit (the white curve) within the reservoir unit and gas hydrate cannot form. In the case of a good seal (the right-hand reservoir), the reservoir can receive methane from the adjacent fines via diffusion (the small blue arrows) or by short- or long-range advection (the large blue arrow). The methane influx (the blue arrows) elevates the pore-water methane concentration (the yellow curve) in the reservoir such that the solubility limit is reached near the base of gas hydrate stability, and gas hydrate can form in the coarse-grained reservoir. Above the reservoir, where the methane concentration meets the solubility limit and effective stresses are lower, gas hydrate-filled fractures can occur in fine-grained sediment. The stepwise solubility change at the coarse-grained/fine-grained interface at the reservoir boundary occurs due to the small pore size in the seal relative to the reservoir (Henry et al., 1999).

Downloaded from https://pubs.geoscienceworld.org/interpretation/article-pdf/doi/10.1190/INT-2019-0026.1/4960317/int-2019-0026.1.pdf?casa_token=CeuYDf8A8V4AAAAA:dcWyYhgKtzGllWkcLSwDi9X2CCPeCCKpldR4zP
by USGS Library user

cores that have had their pressure maintained by methane-free water has been observed to dissolve and disappear (Jang et al., 2019a). At site NGHP-02-09 (Figure 6b), an interval of coarse-grained, reservoir-quality sediment that is seemingly free of gas hydrate (242–248 mbsf) exists between two thick, gas hydrate-filled reservoir sediment intervals. A similar arrangement is noted by Boswell et al. (2012) at Green Canyon Site 955 (GC955) in the Gulf of Mexico. The process by which mid-reservoir bands of limited gas hydrate in coarse-grained sediment occur are not well-known, but Boswell et al. (2012) and Collett et al. (2019) suggest that these water-bearing sands may indicate intervals through which the flow of methane-poor fluid either hampers additional gas hydrate formation or actively dissolves the existing gas hydrate. The continuous presence of methane at or above equilibrium solubility concentrations is critical for gas hydrate to persist.

Extracting methane from a gas hydrate-bearing reservoir

For effective depressurization, the pore-water supply into the production interval has to be limited. In extreme cases, such as what Reagan et al. (2008) define as a "class 2" reservoir where the gas hydrate-bearing reservoir interval is in contact with a permeable, water-bearing sand, water extracted at the well can

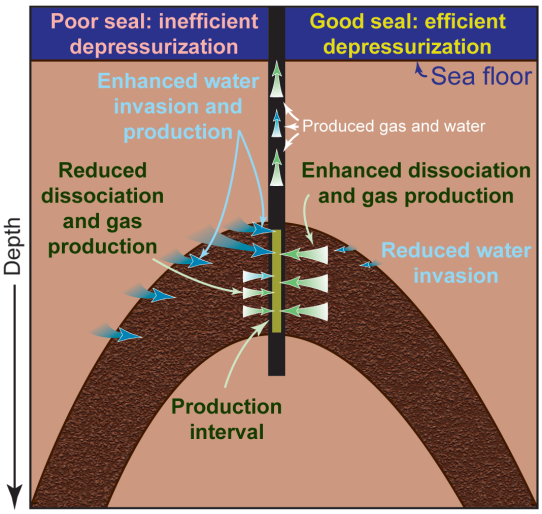

Figure 10. Production efficiency of a gas hydrate reservoir (the stippled arch) depends on whether the reservoir contacts permeable sediment (the left-hand side) or impermeable sediment (the right-hand side). As the pore pressure is drawn down over the production interval, a permeable overburden allows water to invade the reservoir and enter the well (the blue arrows). This water invasion limits the pressure drawdown and, consequently, the driving force for gas hydrate dissociation (Ajayi et al., 2018; Konno et al., 2019). The produced water-to-gas ratio is high relative to the low-permeability overburden case (the right-hand side), where very little water can invade the reservoir. Without water invasion, pore pressure can be drawn down more effectively in the reservoir, enhancing dissociation and gas production rates.

be largely replaced via flow from the water-bearing sand. This inflow limits the pressure reduction imposed on the reservoir; hence, it slows down gas hydrate dissociation and the gas production rate (Reagan et al., 2008; Boswell et al., 2009). As noted by Myshakin et al. (2019), site NGHP-02-16 also appears to have water-bearing sand at the base of the gas hydrate-bearing reservoir. This would limit gas production unless the production interval is isolated from the water-bearing layer.

Even if the site NGHP-02-16 production interval is isolated from the underlying water-bearing layer, the effectiveness of depressurization is limited by the permeability of the overburden seal (Konno et al., 2019). As shown in Figure 10, a permeable overburden can be a source of water entering the reservoir in response to reservoir depressurization, particularly for the large depressurizations (up to 25 MPa) proposed for site NGHP-02-16 (Boswell et al., 2019a; Konno et al., 2019; Myshakin et al., 2019). Based on the site NGHP-02-16 reservoir model by Konno et al. (2019), the peak gas production drops by 25% when the overburden seal permeability is assumed to be 0.1 mD rather than 0.01 mD. Reservoir modeling by Ajayi et al. (2018) for the permafrost gas hydrate reservoir at the Prudhoe Bay "L-pad" indicates that the peak gas production rate drops nearly in half when the overburden seal permeability is assumed as 1 mD rather than the more commonly assumed impermeable limit of 0 mD. Thus, a reliable prediction of a reservoir's gas production rates requires credible properties of the seal sediment, particularly the permeability (Ajayi et al., 2018). These properties can be measured using laboratory experiments with in situ samples. To avoid the sediment-fabric disruption that occurs during gas exsolution even in the absence of gas hydrate, pressure coring and pressure core analysis are recommended for geotechnical testing of in situ seal sediment.

By extension, it is also important to test fine-grained layers that are interbedded in the primary coarse-grained reservoir. These intrareservoir "seals" can help isolate production in particularly favorable portions of the reservoir (Konno et al., 2019; Myshakin et al., 2019) and can help focus depressurization within the coarser grained sediments. Slight variations in clay content may be all that is needed to dramatically alter the gas hydrate saturation in reservoir sediment, or even form essentially gas hydrate-free, intrareservoir interbeds where adjacent layers have significantly different gas hydrate saturations.

The link between clay content and gas hydrate saturation is demonstrated in Figure 11. As the clay content increases (increasing percentage of particles with diameters below 4 μm), the gas hydrate saturation decreases, even in sediment subsamples taken from the gas hydrate-bearing intervals. The dependence of gas hydrate saturation on clay content can be more significant than the dependence on sediment grain size. The R3 specimen, for instance, has a higher d_{50} than R2, but

Downloaded from https://pubs.geoscienceworld.org/interpretation/article-pdf/doi/10.1190/INT-2019-0026.1/4960317/int-2019-0026.1.pdf?casa_token=CeuYDf8A8V4AAAAA:dcWyYhgKtzGllWkcLSwDi9X2CCPeCCKpldR4zP
by USGS Library user

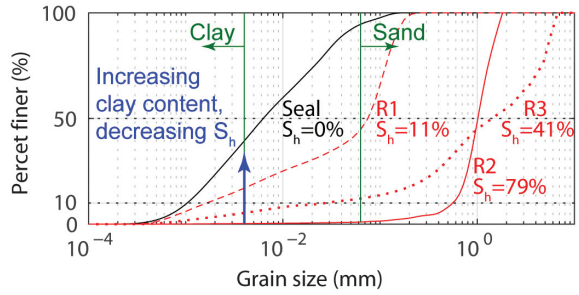

Figure 11. Particle size distributions from site NGHP-02-09 showing the dependence of gas hydrate saturation (S_h) on the content of clay (percentage of particles less than 4 μm in diameter). The clay content can be more important than the median grain size (percent finer = 50, d_{50}) in limiting S_h, as evidenced by comparing R2 and R3. Seal (the black curve): 90.15 mbsf, 36.6% clay, $d_{50} = 6.9$ μm, $S_h = 0\%$. R1 (the dashed red curve): 201.02 mbsf, 15.4% clay, $d_{50} = 58.9$ μm, $S_h = 11\%$. R2 (the solid red curve): 257.26 mbsf, 0.3% clay, $d_{50} = 1112.9$ μm, $S_h = 79\%$. R3 (the dotted red curve): 232.03 mbsf, 4.7% clay, $d_{50} = 1695.2$ μm, $S_h = 41\%$. Data are from Waite et al. (2019a, 2019b).

also has a higher clay content and, consequently, a lower gas hydrate saturation. Quantifying the clay content is important for understanding the gas hydrate reservoir system behavior such as gas hydrate saturation and morphology as well as reservoir permeability and production efficiency. Additional parameters that describe the shape of the grain size distribution curve, such as sorting and the coefficient of uniformity, are also valuable to document.

Conclusion

This study emphasizes the additional system insights that can be gained from considering the fine-grained sediment overlying a coarse-grained gas hydrate-bearing reservoir as a distinct PSs seal element (traditional PS approach), rather than assuming the gas hydrate-bearing reservoir sediment is its own seal (common GHPSs approach). The overlying seal sediment can restrict methane migration out of the coarse-grained reservoir and even contribute methane to help raise the methane concentration enough to form gas hydrate in the coarse sediment. For gas production, the seal sediment can accentuate depressurization in the target reservoir interval and reduce water production during depressurization. Based on the significant, site-specific influences that fine-grained sediments have on the evolution and behavior of the underlying coarse-grained gas hydrate reservoir, a reservoir's overlying fine-grained sediment merits consideration and testing as a distinct seal element in the modified GHPS.

Acknowledgments

This work was supported by the U.S. Geological Survey's Gas Hydrates Project, the Survey's Coastal/Marine Hazards and Resources Program, and by interagency agreements between the U.S. Geological Survey and the Department of Energy (DE-FE0026166 and DE-FE0023495). This report was prepared as an account of work sponsored by an agency of the U.S. government. Any use of trade, firm, or product name is for descriptive purposes only and does not imply endorsement by the U.S. government. The authors thank A. Cook, S. Phillips, C. Ruppel, M. Santra, and an anonymous reviewer for constructive comments on the manuscript. The experimental data are available online in the USGS science database at Jang et al. (2018) and Waite et al. (2018).

Data and materials availability

Data associated with this research are available and can be accessed via the following URL: https://doi.org/10.5066/P91XJ7DP; https://doi.org/10.5066/P97RL4X4.

References

Adolph, B., C. Stoller, M. Archer, D. Codazzi, T. el-Halawani, P. Perciot, G. Weller, M. Evans, J. Grant, R. Griffiths, D. Hartman, G. Sirkin, M. Ichikawa, G. Scott, I. Tribe, and D. White, 2005, No more waiting: Formation evolution while drilling: Oilfield Review, **17**, 4–21.

Ajayi, T., B. J. Anderson, Y. Seol, R. Boswell, and E. M. Myshakin, 2018, Key aspects of numerical analysis of gas hydrate reservoir performance: Alaska North Slope Prudhoe Bay Unit "L-Pad" hydrate accumulation: Journal of Natural Gas Science and Engineering, **51**, 37–43, doi: 10.1016/j.jngse.2017.12.026.

Amer, A. M., and A. A. Awad, 1974, Permeability of cohesionless soils: Journal of Geotechnical Engineering Division, American Society of Civil Engineers, **100**, 1309–1326.

Berner, R. A., 1980, Early diagenesis: A theoretical approach: Princeton University Press.

Boswell, R., and T. S. Collett, 2011, Current perspectives on gas hydrate resources: Energy & Environmental Science, **4**, 1206–1215, doi: 10.1039/c0ee00203h.

Boswell, R., T. S. Collett, M. Frye, W. Shedd, D. R. McConnell, and D. Shelander, 2012, Subsurface gas hydrates in the northern Gulf of Mexico: Marine and Petroleum Geology, **34**, 4–30, doi: 10.1016/j.marpetgeo.2011.10.003.

Boswell, R., E. Myshakin, G. Moridis, Y. Konno, T. S. Collett, M. Reagan, T. Ajayi, and Y. Seol, 2019a, India National Gas Hydrate Program Expedition 02 summary of scientific results: Numerical simulation of reservoir response to depressurization: Marine and Petroleum Geology, **108**, 154–166, doi: 10.1016/j.marpetgeo.2018.09.026.

Boswell, R., K. Rose, T. S. Collett, M. Lee, W. Winters, K. A. Lewis, and W. Agena, 2011, Geologic controls on gas hydrate occurrence in the Mount Elbert prospect, Alaska North Slope: Marine and Petroleum Geology, **28**, 589–607, doi: 10.1016/j.marpetgeo.2009.12.004.

Boswell, R., D. Shelander, M. Lee, T. Latham, T. Collett, G. Guerin, G. Moridis, M. Reagan, and D. Goldberg, 2009, Occurrence of gas hydrate in Oligocene Frio sand:

Downloaded from https://pubs.geoscienceworld.org/interpretation/article-pdf/doi/10.1190/INT-2019-0026.1/4960317/int-2019-0026.1.pdf?casa_token=CeuYDf8A8V4AAAAA:dcWyYhgKtzGllWkcLSwDi9X2CCPeCCKpldR4zP
by USGS Library user

Alaminos Canyon Block 818: Northern Gulf of Mexico: Marine and Petroleum Geology, **26**, 1499–1512, doi: 10.1016/j.marpetgeo.2009.03.005.

Boswell, R., J. Yoneda, and W. F. Waite, 2019b, India National Gas Hydrate Program Expedition 02 summary of scientific results: Evaluation of natural gas hydrate-bearing pressure cores: Marine and Petroleum Geology, **108**, 143–153, doi: 10.1016/j.marpetgeo.2018.1010.1020.

Carrier, W. D., 2003, Goodbye, Hazen; Hello, Kozeny-Carman: Journal of Geotechnical and Geoenvironmental Engineering, **129**, 1054–1056, doi: 10.1061/(Asce)1090-0241(2003)129:11(1054).

Chapuis, R. P., 2004, Predicting the saturated hydraulic conductivity of sand and gravel using effective diameter and void ratio: Canadian Geotechnical Journal, **41**, 787–795, doi: 10.1139/T04-022.

Chong, S. C., Y. T. Liu, M. Cummins, D. L. Valentine, and D. R. Boone, 2002, Methanogenium marinum sp nov., a H-2-using methanogen from Skan Bay, Alaska, and kinetics of H-2 utilization: Antonie Van Leeuwenhoek International Journal of General and Molecular Microbiology, **81**, 263–270, doi: 10.1023/A:1020535222281.

Clennell, M. B., M. Hovland, J. S. Booth, P. Henry, and W. J. Winters, 1999, Formation of natural gas hydrates in marine sediments — 1: Conceptual model of gas hydrate growth conditioned by host sediment properties: Journal of Geophysical Research-Solid Earth, **104**, 22985–23003, doi: 10.1029/1999jb900175.

Collett, T. S., 1995, Gas hydrate resources of the United States, *in* D. L. Gautier, G. L. Dolton, K. I. Takahashi, and K. L. Varnes, eds., National Assessment of United States Oil and Gas Resources: USGS Digital Data Series **30**, CD-ROM.

Collett, T. S., R. Boswell, J. R. Cochran, P. Kumar, M. Lall, A. Mazumdar, M. V. Ramana, T. Ramprasad, M. Riedel, K. Sain, A. V. Sathe, and K. Vishwanath, and NGHP Expedition 01 Science Party, 2014, Geologic implications of gas hydrates in the offshore of India: Results of the National Gas Hydrate Program Expedition 01: Marine and Petroleum Geology, **58**, 3–28, doi: 10.1016/j.marpetgeo.2014.07.021.

Collett, T. S., R. Boswell, W. F. Waite, P. Kumar, S. K. Roy, K. Chopra, S. K. Singh, Y. Yamada, N. Tenma, J. Pohlman, and M. Zyrianova, and the NGHP Expedition 02 Scientific Party, 2019, India National Gas Hydrate Program Expedition 02 summary of scientific results: Gas hydrate systems along the eastern continental margin of India: Marine and Petroleum Geology, **108**, 39–142, doi: 10.1016/j.marpetgeo.2019.05.023.

Collett, T. S., A. H. Johnson, C. C. Knapp, and R. Boswell, 2009, Natural gas hydrates: A review, *in* T. S. Collett, A. H. Johnson, C. C. Knapp, and R. Boswell, eds., Natural gas hydrates — Energy resource potential and associated geologic hazards: AAPG Memoir 89, 146–219.

Collett, T. S., and K. Kvenvolden, 1988, Natural gas hydrate, *in* L. B. Magoon, ed., Petroleum systems of the United States: U.S. Geological Survey Bulletin 1870, 46–47.

Collett, T. S., M. W. Lee, W. F. Agena, J. J. Miller, K. A. Lewis, M. V. Zyrianova, R. Boswell, and T. L. Inks, 2011, Permafrost-associated natural gas hydrate occurrences on the Alaska North Slope: Marine and Petroleum Geology, **28**, 279–294, doi: 10.1016/j.marpetgeo.2009.12.001.

Collett, T. S., M. Riedel, R. Boswell, J. Presley, P. Kumar, A. Sathe, A. Sethi, and M. Lall, and NGHP Expedition Scientists, 2015, Indian National Gas Hydrate Program Expedition 01 report: U.S. Geological Survey, 2012-5054.

Cook, A. E., B. I. Anderson, A. Malinverno, S. Mrozewski, and D. S. Goldberg, 2010, Electrical anisotropy due to gas hydrate-filled fractures: Geophysics, **75**, no. 6, F173–F185, doi: 10.1190/1.3506530.

Cook, A. E., and A. Malinverno, 2013, Short migration of methane into a gas hydrate-bearing sand layer at Walker Ridge, Gulf of Mexico: Geochemistry Geophysics Geosystems, **14**, 283–291, doi: 10.1002/ggge.20040.

D'Hondt, S., B. B. Jorgensen, D. J. Miller, A. Batzke, R. Blake, B. A. Cragg, H. Cypionka, G. R. Dickens, T. Ferdelman, K. U. Hinrichs, N. G. Holm, R. Mitterer, A. Spivack, G. Z. Wang, B. Bekins, B. Engelen, K. Ford, G. Gettemy, S. D. Rutherford, H. Sass, C. G. Skilbeck, I. W. Aiello, G. Guerin, C. H. House, F. Inagaki, P. Meister, T. Naehr, S. Niitsuma, R. J. Parkes, A. Schippers, D. C. Smith, A. Teske, J. Wiegel, C. N. Padilla, and J. L. S. Acosta, 2004, Distributions of microbial activities in deep subseafloor sediments: Science, **306**, 2216–2221, doi: 10.1126/science.1101155.

Dai, S., R. Boswell, W. F. Waite, J. Jang, J. Y. Lee, and Y. Seol, 2017, What has been learned from pressure cores: 9th International Conference on Gas Hydrates.

Dai, S., J. Kim, Y. Xu, W. F. Waite, J. Jang, T. S. Collett, and P. Kumar, 2019, Permeability anisotropy and relative permeability in sediments from the National Gas Hydrate Program Expedition 02, offshore India: Marine and Petroleum Geology, **108**, 705–713, doi: 10.1016/j.marpetgeo.2018.08.016.

Dai, S., C. Lee, and J. C. Santamarina, 2011, Formation history and physical properties of sediments from the Mount Elbert gas hydrate stratigraphic test well, Alaska North slope: Marine and Petroleum Geology, **28**, 427–438, doi: 10.1016/j.marpetgeo.2010.03.005.

Daigle, H., A. Cook, and A. Malinverno, 2018, Formation of massive hydrate deposits in Gulf of Mexico sand layers: Fire in the Ice, **18**, 1–3.

Daigle, H., and B. Dugan, 2010, Origin and evolution of fracture-hosted methane hydrate deposits: Journal of Geophysical Research-Solid Earth, **115**, B11103, doi: 10.1029/2010jb007492.

Dixit, G., H. Ram, and P. Kumar, 2019, Origin of gas in gas hydrates as interpreted from geochemistry data obtained during the National Gas Hydrate Program Expedition 02, Krishna Godavari Basin, offshore India: Marine and Petroleum Geology, **108**, 389–396, doi: 10.1016/j.marpetgeo.2018.11.047.

Downloaded from https://pubs.geoscienceworld.org/interpretation/article-pdf/doi/10.1190/INT-2019-0026.1/4960317/int-2019-0026.1.pdf?casa_token=CeuYDf8A8V4AAAAA:dcWyYhgKtzGllWkcLSwDi9X2CCPeCCKpldR4zP
by USGS Library user

Flemings, P. B., R. Boswell, T. S. Collett, A. E. Cook, D. Divins, M. Frye, G. Guerin, D. S. Goldberg, A. Malinverno, K. Meazell, J. Morrison, T. Pettigrew, S. C. Phillips, M. Santra, D. E. Sawyer, W. Shedd, C. Thomas, and K. You, 2017, GOM2: Prospecting, drilling and sampling coarse-grained hydrate reservoirs in the deepwater Gulf of Mexico: 9th International Conference on Gas Hydrates (ICGH9).

Frye, M., 2008, Preliminary evaluation of in-place gas hydrate resources: Gulf of Mexico Outer Continental Shelf, Minerals Management Service, OCS Report MMS 2008-004, https://www.boem.gov/sites/default/files/documents//MMS2008-004.pdf, accessed 11 February 2020.

Fujii, T., K. Suzuki, T. Takayama, M. Tamaki, Y. Komatsu, Y. Konno, J. Yoneda, K. Yamamoto, and J. Nagao, 2015, Geological setting and characterization of a methane hydrate reservoir distributed at the first offshore production test site on the Daini-Atsumi Knoll in the eastern Nankai Trough, Japan: Marine and Petroleum Geology, **66**, 310–322, doi: 10.1016/j.marpetgeo.2015.02.037.

Grundger, F., V. Carrier, M. M. Svenning, G. Panieri, T. R. Vonnahme, S. Klasek, and H. Nieman, 2019, Methane-fuelled biofilms predominantly composed of methanotrophic ANME-1 in Arctic gas hydrate-related sediments: Scientific Reports, **9**, 9725, doi: 10.1038/s41598-019-46209-5.

Henry, P., M. Thomas, and M. B. Clennell, 1999, Formation of natural gas hydrates in marine sediments — 2: Thermodynamic calculations of stability conditions in porous sediments: Journal of Geophysical Research-Solid Earth, **104**, 23005–23022, doi: 10.1029/1999jb900167.

Holland, M., P. Schultheiss, and J. Roberts, 2019, Gas hydrate concentration and morphology from analysis of pressure cores acquired in the Bay of Bengal during Expedition NGHP-02, offshore India: Marine and Petroleum Geology, **108**, 407–423, doi: 10.1016/j.marpetgeo.2018.07.018.

Hyndman, R. D., and E. E. Davis, 1992, A mechanism for the formation of methane hydrate and sea-floor bottom-simulating reflectors by vertical fluid expulsion: Journal of Geophysical Research-Solid Earth, **97**, 7025–7041, doi: 10.1029/91jb03061.

Ijiri, A., S. Haraguchi, F. J. Jimenez-Espejo, N. Komai, H. Suga, M. Kinoshita, F. Inagaki, and Y. Yamada, 2019, Origin of low-chloride fluid in sediments from the eastern continental margin of India, results from the National Gas Hydrate Program Expedition 02: Marine and Petroleum Geology, **108**, 377–388, doi: 10.1016/j.marpetgeo.2018.06.014.

Jain, A. K., and R. Juanes, 2009, Preferential mode of gas invasion in sediments: Grain-scale mechanistic model of coupled multiphase fluid flow and sediment mechanics: Journal of Geophysical Research-Solid Earth, **114**, B08101, doi: 10.1029/2008jb006002.

Jang, J., S. Dai, J. Yoneda, W. F. Waite, T. S. Collett, and P. Kumar, 2018, Pressure core characterization tool measurements of compressibility, permeability, and shear strength of fine-grained sediment collected from area C, Krishna-Godavari Basin, during India's National Gas Hydrate Program Expedition NGHP-02, https://doi.org/10.5066/P91XJ7DP, accessed 31 December 2018.

Jang, J., S. Dai, J. Yoneda, W. F. Waite, L. Stern, L. Boze, T. S. Collett, and P. Kumar, 2019a, Pressure core analysis on geomechanical and fluid flow properties of a seal layer from the Krishna-Godavari Basin, offshore India: Marine and Petroleum Geology, **108**, 537–550, doi: 10.1016/j.marpetgeo.2018.08.015.

Jang, J., W. F. Waite, L. Stern, T. S. Collett, and P. Kumar, 2019b, Physical property characteristics of gas hydrate-bearing reservoir and associated seal sediments collected during NGHP-02 in the Krishna-Godavari Basin, in the offshore of India: Marine and Petroleum Geology, **108**, 249–271, doi: 10.1016/j.marpetgeo.2018.09.027.

Johnson, A. H., 2011, Global resource potential of gas hydrate — A new calculation: 7th International Conference on Gas Hydrates (ICGH 2011).

Katayama, T., H. Yoshioka, H. A. Takahashi, M. Amo, T. Fujii, and S. Sakata, 2016, Changes in microbial communities associated with gas hydrates in subseafloor sediments from the Nankai Trough: Fems Microbiology Ecology, **92**, fiw093, doi: 10.1093/femsec/fiw093.

Kida, M., Y. Jin, J. Yoneda, M. Oshima, A. Kato, Y. Konno, J. Nagao, and N. Tenma, 2019, Crystallographic and geochemical properties of natural gas hydrates accumulated in the National Gas Hydrate Program Expedition 02 drilling sites in the Krishna-Godavari Basin off India: Marine and Petroleum Geology, **108**, 471–481, doi: 10.1016/j.marpetgeo.2018.10.012.

Kinoshita, M., A. Ijiri, S. Haraguchi, F. J. Jimenez-Espejo, N. Komai, H. Suga, T. Sugihara, W. Tanikawa, T. Hirose, Y. Hamada, L. P. Gupta, N. Ahagon, Y. Masaki, N. Abe, H. Y. Wu, S. Nomura, W. Lin, Y. Yamamoto, and Y. Yamada, 2019, Constraints on the fluid supply rate into and through gas hydrate reservoir systems as inferred from pore-water chloride and in situ temperature profiles, Krishna-Godavari Basin, India: Marine and Petroleum Geology, **108**, 368–376, doi: 10.1016/j.marpetgeo.2018.12.049.

Konno, Y., A. Kato, J. Yoneda, M. Oshima, M. Kida, Y. Jin, J. Nagao, and N. Tenma, 2019, Numerical analysis of gas production potential from a gas-hydrate reservoir at site NGHP-02-16, the Krishna-Godavari basin offshore India — Feasibility of depressurization method for ultra-deepwater environment: Marine and Petroleum Geology, **108**, 731–740, doi: 10.1016/j.marpetgeo.2018.08.001.

Konno, Y., J. Yoneda, K. Egawa, T. Ito, Y. Jin, M. Kida, K. Suzuki, T. Fujii, and J. Nagao, 2015, Permeability of sediment cores from methane hydrate deposit in the Eastern Nankai Trough: Marine and Petroleum Geology, **66**, 487–495, doi: 10.1016/j.marpetgeo.2015.02.020.

Kraemer, L. M., R. M. Owen, and G. R. Dickens, 2000, Lithology of the upper gas hydrate zone, Blake Outer Ridge: A link between diatoms, porosity, and gas hydrate, *in* C. K. Paull, R. Matsumoto, P. J. Wallace, and W. P.

Downloaded from https://pubs.geoscienceworld.org/interpretation/article-pdf/doi/10.1190/INT-2019-0026.1/4960317/int-2019-0026.1.pdf?casa_token=CeuYDf8A8V4AAAAA:dcWyYhgKtzGllWkcLSwDi9X2CCPeCCKpldR4zP
by USGS Library user

Dillon, eds., Proceedings of the Ocean Drilling Program, Scientific Results 164, 229–236.
Kumar, P., T. S. Collett, K. M. Shukla, U. S. Yadav, M. V. Lall, and K. Vishwanath, and NGHP-02 Expedition Scientific Party, 2019, India National Gas Hydrate Program Expedition-02: Operational and technical summary: Marine and Petroleum Geology, **108**, 3–38, doi: 10.1016/j.marpetgeo.2018.11.021.
Kvenvolden, K. A., 1993, Gas hydrates — Geological perspective and global change: Reviews of Geophysics, **31**, 173–187, doi: 10.1029/93rg00268.
Kvenvolden, K. A., and L. A. Barnard, 1983, Gas hydrates of the Blake Outer Ridge. Site 533. Deep Sea Drilling Project Leg 76, *in* R. E. Sheridan and F. M. Gradstein, eds., Initial Reports of the Deep Sea Drilling Project: Deep Sea Drilling Project Reports and Publications, 353–365.
Liu, X. L., and P. B. Flemings, 2006, Passing gas through the hydrate stability zone at southern Hydrate Ridge, offshore Oregon: Earth and Planetary Science Letters, **241**, 211–226, doi: 10.1016/j.epsl.2005.10.026.
Liu, X. L., and P. B. Flemings, 2007, Dynamic multiphase flow model of hydrate formation in marine sediments: Journal of Geophysical Research-Solid Earth, **112**, B03101, doi: 10.1029/2005jb004227.
Liu, X. L., and P. B. Flemings, 2011, Capillary effects on hydrate stability in marine sediments: Journal of Geophysical Research-Solid Earth, **116**, B07102, doi: 10.1029/2010jb008143.
Magoon, L. B., 1988, The petroleum system — A classification scheme for research, exploration, and resource assessment, *in* L. B. Magoon, ed., Petroleum systems of the United States: U.S. Geological Survey Bulletin 1870, 2–15.
Malinverno, A., 2010, Marine gas hydrates in thin sand layers that soak up microbial methane: Earth and Planetary Science Letters, **292**, 399–408, doi: 10.1016/j.epsl.2010.02.008.
Marchesi, J. R., A. J. Weightman, B. A. Cragg, R. J. Parkes, and J. C. Fry, 2001, Methanogen and bacterial diversity and distribution in deep gas hydrate sediments from the Cascadia margin as revealed by 16S rRNA molecular analysis: FEMS Microbiology Ecology, **34**, 221–228, doi: 10.1016/S0168-6496(00)00099-4.
Matsumoto, R., M. Tanahashi, Y. Kakuwa, G. Snyder, S. Ohikawa, H. Tomaru, and S. Morita, 2017, Recovery of thick deposits of massive hydrates from gas chimney structures, eastern margin of Japan Sea: Japan sea shallow gas hydrate project: Fire in the Ice, **17**, 1–6.
Max, M. D., and A. H. Johnson, 2014, Hydrate petroleum system approach to natural gas hydrate exploration: Petroleum Geoscience, **20**, 187–199, doi: 10.1144/petgeo2012-049.
Meyer, D. W., P. B. Flemings, D. DiCarlo, K. H. You, S. C. Phillips, and T. J. Kneafsey, 2018, Experimental investigation of gas flow and hydrate formation within the hydrate stability zone: Journal of Geophysical Research-Solid Earth, **123**, 5350–5371, doi: 10.1029/2018jb015748.
Moridis, G. J., M. T. Reagan, A. F. Queiruga, and R. Boswell, 2019, Evaluation of the performance of the oceanic hydrate accumulation at site NGHP-02-09 in the Krishna-Godavari Basin during a production test and during single and multi-well production scenarios: Marine and Petroleum Geology, **108**, 660–696, doi: 10.1016/j.marpetgeo.2018.12.001.
Myshakin, E., J. S. Lin, S. Uchida, Y. Seol, T. Collett, and R. Boswell, 2019, Numerical simulation of depressurization-induced gas production from an interbedded turbidite hydrate-bearing sedimentary section in the offshore of India: Site NGHP-02-16 (Area-B): Marine and Petroleum Geology, **108**, 619–638, doi: 10.1016/j.marpetgeo.2018.10.047.
Nimblett, J., and C. Ruppel, 2003, Permeability evolution during the formation of gas hydrates in marine sediments: Journal of Geophysical Research, **108**, 2420, doi: 10.1029/2001JB001650.
Nole, M., H. Daigle, A. E. Cook, J. I. T. Hillman, and A. Malinverno, 2017, Linking basin-scale and pore-scale gas hydrate distribution patterns in diffusion-dominated marine hydrate systems: Geochemistry Geophysics Geosystems, **18**, 653–675, doi: 10.1002/2016gc006662.
Paull, C. K., W. Ussler, III, and W. S. Borowski, 1994, Sources of biogenic methane to form marine gas hydrate: Annals of the New York Academy of Science, **715**, 392–409, doi: 10.1111/j.1749-6632.1994.tb38852.x.
Priest, J. A., M. Druce, J. Roberts, P. Schultheiss, Y. Nakatsuka, and K. Suzuki, 2015, PCATS Triaxial: A new geotechnical apparatus for characterizing pressure cores from the Nankai Trough, Japan: Marine and Petroleum Geology, **66**, 460–470, doi: 10.1016/j.marpetgeo.2014.12.005.
Priest, J. A., J. L. Hayley, W. E. Smith, P. Schultheiss, and J. Roberts, 2019, PCATS triaxial testing: Geomechanical properties of sediments from pressure cores recovered from the Bay of Bengal during expedition NGHP-02: Marine and Petroleum Geology, **108**, 424–438, doi: 10.1016/j.marpetgeo.2018.07.005.
Radhakrishna, M., D. Twinkle, S. Nayak, R. Bastia, and G. S. Rao, 2012, Crustal structure and rift architecture across the Krishna-Godavari basin in the central eastern continental margin of India based on analysis of gravity and seismic data: Marine and Petroleum Geology, **37**, 129–146, doi: 10.1016/j.marpetgeo.2012.05.005.
Reagan, M. T., G. Moridis, and K. Zhang, 2008, Sensitivity analysis of gas production from Class 2 and Class 3 hydrate deposits: Offshore Technology Conference.
Rempel, A. W., and B. A. Buffett, 1997, Formation and accumulation of gas hydrate in porous media: Journal of Geophysical Research-Solid Earth, **102**, 10151–10164, doi: 10.1029/97jb00392.
Ren, X. W., and J. C. Santamarina, 2018, The hydraulic conductivity of sediments: A pore size perspective: Engineering Geology, **233**, 48–54, doi: 10.1016/j.enggeo.2017.11.022.
Ryu, B. J., M. Riedel, J. H. Kim, R. D. Hyndman, Y. J. Lee, B. H. Chung, and I. S. Kim, 2009, Gas hydrates in the

Downloaded from https://pubs.geoscienceworld.org/interpretation/article-pdf/doi/10.1190/INT-2019-0026.1/4960317/int-2019-0026.1.pdf?casa_token=CeuYDf8A8V4AAAAA:dcWyYhgKtzGllWkcLSwDi9X2CCPeCCKpldR4zP
by USGS Library user

western deep-water Ulleung Basin, East Sea of Korea: Marine and Petroleum Geology, **26**, 1483–1498, doi: 10.1016/j.marpetgeo.2009.02.004.

Saito, S., K. H. Hsiung, Y. Sanada, K. Moe, Y. Hamada, Y. Nakamura, H. Y. Wu, Y. Shinmoto, and Y. Yamada, and NGHP Expedition 02 JAMSTEC Science Team, 2019, Gas hydrate occurrence and distribution controlled by regional geological structure off eastern India: Estimates from logging-while-drilling in Area-B, National Gas Hydrate Program Expedition 02 (NGHP-02): Marine and Petroleum Geology, **108**, 216–225, doi: 10.1016/j.marpetgeo.2018.12.050.

Santamarina, J. C., S. Dai, J. Jang, and M. Terzariol, 2012, Pressure core characterization tools for hydrate-bearing sediments: Scientific Drilling Journal, **14**, 44–48, doi: 10.2204/iodp.sd.14.06.2012.

Santamarina, J. C., S. Dai, M. Terzariol, J. Jang, W. F. Waite, W. J. Winters, J. Nagao, J. Yoneda, Y. Konno, T. Fujii, and K. Suzuki, 2015, Hydro-bio-geomechanical properties of hydrate-bearing sediments from Nankai Trough: Marine and Petroleum Geology, **66**, 434–450, doi: 10.1016/j.marpetgeo.2015.02.033.

Shukla, K. M., P. Kumar, and U. S. Yadav, and NGHP-02 Science Team, 2019a, Gas hydrate reservoir identification, delineation, and characterization in the Krishna-Godavari basin using subsurface geologic and geophysical data from the National Gas Hydrate Program 02 expedition, offshore India: Marine and Petroleum Geology, **108**, 185–205, doi: 10.1016/j.marpetgeo.2018.10.019.

Shukla, K. M., U. S. Yadav, P. Kumar, T. S. Collett, R. Boswell, M. Frye, M. Riedel, I. Kaur, and K. Vishwanath, 2019b, National Gas Hydrate Program Expedition 02: Identification of gas hydrate prospects in the Krishna-Godavari Basin, offshore India: Marine and Petroleum Geology, **108**, 167–184, doi: 10.1016/j.marpetgeo.2018.11.013.

Singh, R. J., 2014, Exploration application of seismic amplitude analysis in the Krishna-Godavari Basin, east coast of India: Interpretation, **2**, no. 4, SP5–SP20, doi: 10.1190/INT-2013-0197.1.

Sloan, E. D., and C. A. Koh, 2007, Clathrate hydrates of natural gases: CRC Press, Taylor & Francis Group, LLC.

Spinelli, G. A., E. R. Giambalvo, and A. Fisher, 2004, Sediment permeability, distribution, and influence on fluxes in oceanic basement, *in* E. E. Davis and H. Elderfield, eds., Hydrogeology of the oceanic lithosphere: Cambridge University Press, 151–188.

Tripathi, R., P. Kumar, S. Ghosh, J. Nagalingam, and H. Singh, 2019, Culture based investigations of key microbial functional groups in gas hydrate bearing sediments of the Krishna-Godavari Basin in offshore India: Marine and Petroleum Geology, **108**, 397–406, doi: 10.1016/j.marpetgeo.2019.01.034.

Uchida, T., A. Waseda, and T. Namikawa, 2009, Methane accumulation and high concentration of gas hydrate in marine and terrestrial sandy sediments, *in* T. Collett, A. Johnson, C. Knapp, and R. Boswell, eds., Natural gas hydrates — Energy resource potential and associated geologic hazard: AAPG Memoir 89, 401–413.

Ulmishek, G. F., 1988, Types of seals as related to migration and entrapment of hydrocarbons, *in* L. B. Magoon, ed., Petroleum systems of the United States: U.S. Geological Survey, 39–40.

Waite, W. F., J. Jang, T. S. Collett, and P. Kumar, 2018, Grain-size data from India's National Gas Hydrate Program NGHP-02 expedition in the Krishna-Godavari Basin offshore eastern India, 2015: U. S. Geological Survey data release, https://doi.org/10.5066/P97RL4X4, accessed 31 December 2018.

Waite, W. F., J. Jang, T. S. Collett, and P. Kumar, 2019a, Downhole physical properties-based description of a gas hydrate petroleum system in NGHP-02 Area C: A channel, levee, fan complex in the Krishna-Godavari Basin offshore eastern India: Marine and Petroleum Geology, **108**, 272–295, doi: 10.1016/j.marpetgeo.2018.05.021.

Waite, W. F., C. D. Ruppel, T. S. Collett, P. Schultheiss, M. Holland, K. M. Shukla, and P. Kumar, 2019b, Multi-measurement approach for establishing the base of gas hydrate stability in the Krishna-Godavari Basin, offshore India, for sites cored during expedition NGHP-02: Marine and Petroleum Geology, **108**, 296–320, doi: 10.1016/j.marpetgeo.2018.07.026.

Wallmann, K., E. Pinero, E. Burwicz, M. Haeckel, C. Hensen, A. Dale, and L. Ruepke, 2012, The global inventory of methane hydrate in marine sediments: A theoretical approach: Energies, **5**, 2449–2498, doi: 10.3390/en5072449.

Wellsbury, P., K. Goodman, T. Barth, B. A. Cragg, S. P. Barnes, and R. J. Parkes, 1997, Deep marine biosphere fuelled by increasing organic matter availability during burial and heating: Nature, **388**, 573–576, doi: 10.1038/41544.

Xu, W. Y., and C. Ruppel, 1999, Predicting the occurrence, distribution, and evolution of methane gas hydrate in porous marine sediments: Journal of Geophysical Research-Solid Earth, **104**, 5081–5095, doi: 10.1029/1998jb900092.

Yoneda, J., M. Oshima, M. Kida, A. Kato, Y. Konno, Y. Jin, J. Jang, W. F. Waite, P. Kumar, and N. Tenma, 2019, Permeability variation and anisotropy of gas hydrate-bearing pressure-core sediments recovered from the Krishna–Godavari Basin, offshore India: Marine and Petroleum Geology, **108**, 524–536, doi: 10.1016/j.marpetgeo.2018.07.006.

Yoshioka, H., A. Maruyama, T. Nakamura, Y. Higashi, H. Fuse, S. Sakata, and D. H. Bartlett, 2010, Activities and distribution of methanogenic and methane-oxidizing microbes in marine sediments from the Cascadia Margin: Geobiology, **8**, 223–233, doi: 10.1111/j.1472-4669.2009.00231.x.

You, K., P. B. Flemings, A. Malinverno, T. S. Collett, and K. Darnell, 2019, Mechanisms of methane hydrate formation in geological systems: Reviews of Geophysics, **57**, 1146–1196, doi: 10.1029/2018rg000638.

Downloaded from https://pubs.geoscienceworld.org/interpretation/article-pdf/doi/10.1190/INT-2019-0026.1/4960317/int-2019-0026.1.pdf?casa_token=CeuYDf8A8V4AAAAA:dcWyYhgKtzGllWkcLSwDi9X2CCPeCCKpldR4zP
by USGS Library user

You, K. H., and P. B. Flemings, 2018, Methane hydrate formation in thick sand reservoirs — 1: Short-range methane diffusion: Marine and Petroleum Geology, **89**, 428–442, doi: 10.1016/j.marpetgeo.2017.10.011.

Zatsepina, O. Y., and B. A. Buffett, 1997, Phase equilibrium of gas hydrate: Implications for the formation of hydrate in the deep sea floor: Geophysical Research Letters, **24**, 1567–1570, doi: 10.1029/97gl01599.

Biographies and photographs of the authors are not available.

Downloaded from https://pubs.geoscienceworld.org/interpretation/article-pdf/doi/10.1190/INT-2019-0026.1/4960317/int-2019-0026.1.pdf?casa_token=CeuYDf8A8V4AAAAA:dcWyYhgKtzGllWkcLSwDi9X2CCPeCCKpldR4zP
by USGS Library user